
CHAPTER 8

Light-Induced Nanostructure Formation using Azobenzene Polymers

Kevin G. Yager, Christopher J. Barrett

Department of Chemistry, McGill University, Montreal, QC, Canada, H3A 2K6

CONTENTS

1. Introduction	1
2. Azobenzene	2
2.1. Azobenzene Chromophores	2
2.2. Azobenzene Photochemistry	3
2.3. Azobenzene Systems	5
3. Photoinduced Motions and Modulations	10
3.1. Molecular Motion	10
3.2. Photo Orientation	10
3.3. Domain Motion	13
3.4. Micrometer-Scale Motion	14
3.5. Macroscopic Motion	14
3.6. Other Applications of Azobenzenes	15
4. Surface Mass Transport	16
4.1. Experimental Observations	18
4.2. Mechanism	25
4.3. Applications of Surface Mass Transport	29
5. Conclusions	30
References	30

1. INTRODUCTION

The formation of useful nanostructures, and interfacing these with macro-world devices, is an ongoing research challenge. The microelectronics industry has a wide variety of optical tools available for patterning using light and has achieved remarkable control over material properties. It is therefore attractive to investigate future patterning techniques that take advantage of this visible-light lithographic infrastructure. Azobenzene molecules exhibit numerous photoresponsive properties, which can be exploited to locally modify material properties.

Specifically, irradiation of azobenzenes with light causes a fast and efficient change of the molecule's configuration. This photoisomerization can be exploited as a photoswitch, to orient the chromophore (which induces birefringence) or even to perform all-optical surface topography patterning. These photo-motions enable many interesting applications, ranging from optical components and lithography to sensors and smart materials.

This chapter will discuss the many unique properties of the azobenzene chromophore and the exceptional material control enabled when these chromophores are incorporated in a polymeric matrix. More specifically, we will attempt to highlight the ways in which azo-polymers could be used as tools in the emerging field of controlled nanostructure formation.

2. AZOBENZENE

Azobenzene is an aromatic molecule formed by an azo linkage ($-\text{N}=\text{N}-$) connecting two phenyl rings. In this text, as in most on the subject, we use "azobenzene" and "azo" in a more general way: to refer to the class of compounds that exhibit the core azobenzene structure, with different ring substitution patterns (even though, strictly, these compounds should be referred to as "diazenes"). There are many properties common to nearly all azobenzene molecules. The most obvious is the strong electronic absorption of the conjugated π -system. The absorption spectrum can be tailored, via the ring substitution pattern, to lie anywhere from the ultraviolet to the visible-red region. It is not surprising that azobenzenes were originally used as dyes and colorants [1, 2]. The geometrically rigid structure and large aspect ratio of azobenzene molecules make them ideal mesogens: azobenzene small molecules and polymers functionalized with azobenzene can exhibit liquid-crystalline phases [3, 4]. The most startling and intriguing characteristic of the azobenzenes is their highly efficient and fully reversible photoisomerization. Azobenzenes have two stable isomeric states: a thermally stable trans configuration and a metastable cis form. Remarkably, the azo chromophore can interconvert between these isomers upon absorption of a photon. For most azobenzenes, the molecule can be optically isomerized from trans to cis with light anywhere within the broad absorption band, and the molecule will subsequently thermally relax back to the trans state on a timescale dictated by the substitution pattern. This clean photochemistry is central to azobenzene's potential use as a tool for nanopatterning.

2.1. Azobenzene Chromophores

Azobenzenes can be separated into three spectroscopic classes, well described by Rau: [5] azobenzene-type molecules, aminoazobenzene-type molecules, and pseudo-stilbenes (refer to Fig. 1 for examples). The particulars of their absorption spectra (shown in Fig. 2) give rise to their prominent colors: yellow, orange, and red, respectively. Many azos exhibit absorption characteristics similar to those of the unsubstituted azobenzene archetype. These molecules exhibit a low-intensity $n \rightarrow \pi^*$ band in the visible region, and a much stronger $\pi \rightarrow \pi^*$

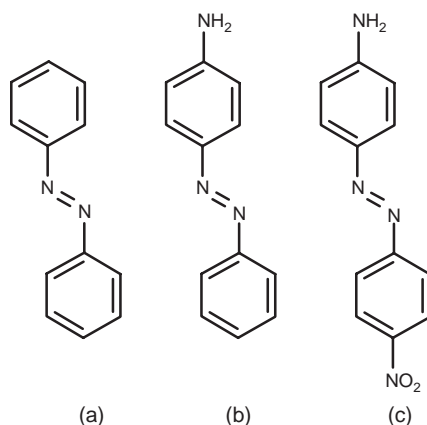


Figure 1. Examples of azo molecules classified as (a) azobenzenes, (b) aminoazobenzenes, and (c) pseudo-stilbenes.

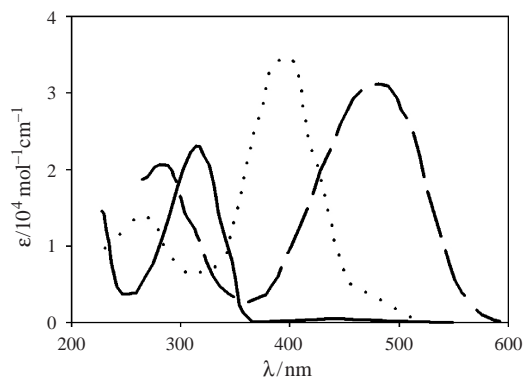


Figure 2. Schematic of typical absorbance spectra for *trans*-azobenzenes. The azobenzene-type molecules (solid line) have a strong absorption in the UV, and a low-intensity band in the visible (barely visible in the graph). The aminoazobenzenes (dotted line) and pseudo-stilbenes (dashed line) typically have strong overlapped absorptions in the visible region.

band in the UV. Although the $n \rightarrow \pi^*$ is symmetry-forbidden for *trans*-azobenzene (C_{2h}), vibrational coupling and some extent of nonplanarity make it nevertheless observable [6].

Adding substituents to the azobenzene rings may lead to minor or major changes in spectroscopic character. Of particular interest is ortho- or para-substitution with an electron-donating group (usually an amino, $-\text{NH}_2$), which results in a new class of compounds. In these aminoazobenzenes, the $n \rightarrow \pi^*$ and $\pi \rightarrow \pi^*$ bands are much closer. In fact, the $n \rightarrow \pi^*$ may be completely buried beneath the intense $\pi \rightarrow \pi^*$. Whereas azobenzenes are fairly insensitive to solvent polarity, aminoazobenzene absorption bands shift to higher energy in nonpolar solvents and shift to lower energy in polar solvents. Substituting azobenzene at the 4- and 4'-positions with an electron-donor and an electron-acceptor (such as an amino and a nitro, $-\text{NO}_2$, group) leads to a strongly asymmetric electron distribution (often referred to as a “push/pull” substitution pattern). This shifts the $\pi \rightarrow \pi^*$ absorption to lower energy, toward the red and past the $n \rightarrow \pi^*$. This reversed ordering of the absorption bands defines the third spectroscopic class, the pseudo-stilbenes (in analogy to stilbene, phenyl—C=C—phenyl). The pseudo-stilbenes are very sensitive to local environment, which can be useful in some applications.

Especially in condensed phases, the azos are also sensitive to packing and aggregation. The π - π stacking gives rise to shifts of the absorption spectrum. If the azo dipoles have a parallel (head-to-head) alignment, they are called J-aggregates and give rise to a red shift of the spectrum (bathochromic) as compared to the isolated chromophore. If the dipoles are antiparallel (head-to-tail), they are called H-aggregates and lead to a blue shift (hypsochromic). Fluorescence is seen in some aminoazobenzenes and many pseudo-stilbenes, but not in azobenzenes, whereas phosphorescence is absent in all three classes. By altering the electron density, the substitution pattern necessarily affects the dipole moment, and in fact all the higher-order multipole moments. This becomes significant in many nonlinear optical (NLO) studies. For instance, the chromophore’s dipole moment can be used to orient with an applied electric field (poling), and the higher order moments of course define the molecule’s nonlinear response [7]. In particular, the strongly asymmetric distribution of the delocalized electrons that results from push/pull substitution results in an excellent NLO chromophore.

2.2. Azobenzene Photochemistry

Key to some of the most intriguing results and interesting applications of azobenzenes is the facile and reversible photoisomerization about the azo bond, converting between the *trans* (E) and *cis* (Z) geometric isomers (Fig. 3). This photoisomerization is completely reversible and free from side reactions, prompting Rau to characterize it as “one of the cleanest photoreactions known” [5]. The *trans* isomer is more stable by approximately 50 kJ/mol [8, 9], and the energy barrier to the photo-excited state (barrier to isomerization) is on the order

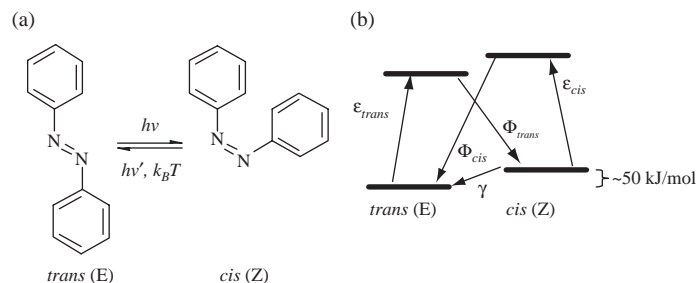


Figure 3. (a) Azobenzene can convert between *trans* and *cis* states photochemically, and relaxes to the more stable *trans* state thermally. (b) Simplified state model for azobenzenes. The *trans* and *cis* extinction coefficients are denoted ϵ_{trans} and ϵ_{cis} . The Φ refer to quantum yields of photoisomerization, and γ is the thermal relaxation rate constant.

of 200 kJ/mol [10]. Thus, in the dark, most azobenzene molecules will be found in the *trans* form. Upon absorption of a photon (with a wavelength in the *trans* absorption band), the azobenzene will convert, with high efficiency, into the *cis* isomer. A second wavelength of light (corresponding to the *cis* absorption band) can cause the back-conversion. These photoisomerizations usually have picosecond timescales [11, 12]. Alternately, azos will thermally reconvert from the *cis* to *trans* state, with a timescale ranging from milliseconds to hours, depending on the substitution pattern and local environment. More specifically, the lifetimes for azobenzenes, aminoazobenzenes, and pseudo-stilbenes are usually on the order of hours, minutes, and seconds, respectively. In some cases, bulky substituents can inhibit the *cis* \rightarrow *trans* relaxation process, thereby allowing the *cis* state to persist for days. For instance, a polyurethane with the azo chromophore in the main chain exhibited a thermal rate constant of $2.8 \times 10^{-6} \text{ s}^{-1}$ (at 3°C) [13], and an azobenzene with bulky pendant groups had a rate constant $< 2 \times 10^{-7} \text{ s}^{-1}$ (at room temperature) [14]. It is also possible to prevent the *cis* \rightarrow *trans* isomerization entirely by adsorption to a surface [15] or synthesizing constrained (usually ringlike) molecules [16]. It is also worth noting that the *cis* form of the parent azobenzene can in fact be stabilized and isolated by crystallization [17, 18].

A bulk azo sample or solution under illumination will achieve a photostationary state, with a steady-state *trans/cis* composition based on the competing effects of photoisomerization into the *cis* state, thermal relaxation back to the *trans* state, and possibly *cis* reconversion upon light absorption. The steady-state composition is unique to each system, as it depends on the quantum yields for the two processes (Φ_{trans} and Φ_{cis}) and the thermal relaxation rate constant. The composition also depends upon irradiation intensity, wavelength, temperature, and the matrix (gas phase, solution, liquid crystal, sol-gel, monolayer, polymer matrix, etc.). Azos are photochromic (their color changes upon illumination), since the effective absorption spectrum (a combination of the *trans* and *cis* spectra) changes with light intensity. Thus absorption spectroscopy can be conveniently used to measure the *cis* fraction in the steady state [19, 20] and the subsequent thermal relaxation to an all-*trans* state [21–24]. Under moderate irradiation, the composition of the photostationary state is predominantly *cis* for azobenzenes, mixed for aminoazobenzenes, and predominantly *trans* for pseudo-stilbenes. In the dark, the *cis* fraction is below most detection limits, and the sample can be considered to be in an all-*trans* state. Isomerization is induced by irradiating with a wavelength within the azo's absorption spectrum, preferably close to λ_{max} . Modern experiments typically use laser excitation with polarization control, delivering on the order of 1–100 mW/cm² of power to the sample. Various lasers cover the spectral range of interest, from the UV (Ar⁺ line at 350 nm), through blue (Ar⁺ at 488 nm) and green (Ar⁺ at 514 nm, YAG at 532 nm, HeNe at 545 nm) and into the red (HeNe at 633 nm, GaAs at 675 nm).

The ring substitution pattern affects both the *trans* and the *cis* absorption spectra, and for certain patterns, the absorption spectra of the two isomers overlap significantly (notably for the pseudo-stilbenes). In these cases, a single wavelength of light effectuates both the forward and reverse reaction, leading to a mixed stationary state and continual interconversion of the molecules. For some interesting azobenzene photo-motions, this rapid and efficient cycling of chromophores is advantageous, whereas in cases where the azo chromophore is being used as a switch, it is clearly undesirable.

The mechanism of isomerization has undergone considerable debate. Isomerization takes place either through a rotation about the N—N bond, with rupture of the π bond, or through inversion, with a semilinear and hybridized transition state, where the π bond remains intact (refer to Fig. 4). The thermal back-relaxation is agreed to be via rotation, whereas for the photochemical isomerization, both mechanisms appear viable [25]. Historically the rotation mechanism (as necessarily occurs in stilbene) was favored for photoisomerization, with some early hints that inversion may be contributing [26]. More recent experiments, based on matrix or molecular constraints to the azobenzene isomerization, strongly support inversion [27–30]. Studies using picosecond Raman and femtosecond fluorescence show a double bond (N=N) in the excited state, confirming the inversion mechanism [31, 32]. By contrast, Ho et al. [33] found evidence that the pathway is compound-specific: a nitro-substituted azobenzene photoisomerized via the rotation pathway. Furthermore, *ab initio* and density functional theory calculations indicate that both pathways are energetically accessible, although inversion is preferred [34, 35]. Thus, both mechanisms may be competing, with a different one dominating depending on the particular chromophore and environment. The emerging consensus nevertheless appears to be that inversion is the dominant pathway for most azobenzenes [36]. The availability of the inversion mechanism explains how azos are able to isomerize easily even in rigid matrices, such as glassy polymers, since the inversion mechanism has a much smaller free volume requirement than the rotation.

The thermal back-relaxation is generally first-order, although a glassy polymer matrix can lead to anomalously fast decay components [37–40], attributed to a distribution of chromophores in highly strained configurations. Higher matrix crystallinity increases the rate of decay [41]. The decay rate itself can act as a probe of local environment and molecular conformation [42, 43]. The back-relaxation of azobenzene is acid-catalyzed [44], although strongly acidic conditions will lead to side-reactions [18]. For the parent azobenzene molecule, quantum yields (which can be indirectly measured spectroscopically [37, 45, 46]) are on the order of 0.6 for the trans \rightarrow cis photoconversion and 0.25 for the back photoreaction. Solvent has a small effect, increasing the trans \rightarrow cis and decreasing the cis \rightarrow trans yield as polarity increases [47]. Aminoazobenzenes and pseudo-stilbenes isomerize very quickly and can have quantum yields as high as 0.7–0.8.

2.3. Azobenzene Systems

Azobenzenes are robust and versatile moieties and have been extensively investigated as small molecules, as pendants on other molecular structures, or incorporated (doped or covalently bound) into a wide variety of amorphous, crystalline, or liquid crystalline polymeric

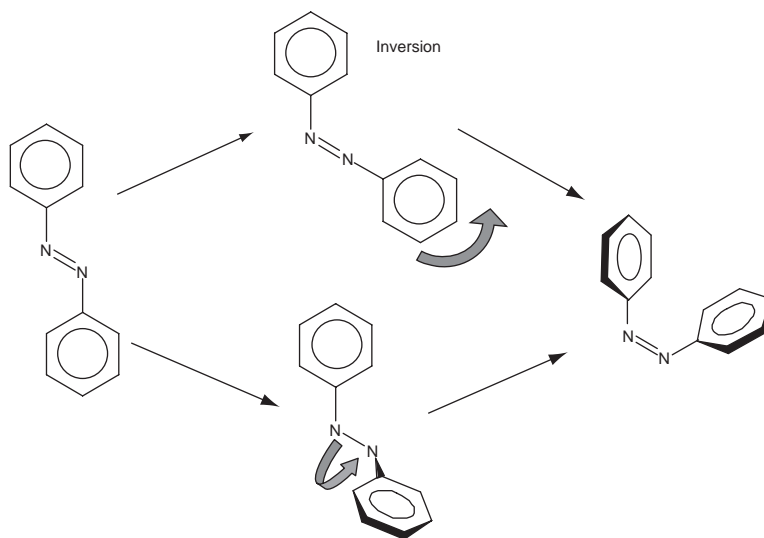


Figure 4. The mechanism of azobenzene isomerization proceeds either via rotation or inversion. The *cis* state has the phenyl rings tilted at 90° with respect to the CNNC plane.

systems. Noteworthy examples include self-assembled monolayers and superlattices [48], sol-gel silica glasses [49], and biomaterials [50–52]. A number of small molecules incorporating azobenzene have been synthesized, including crown ethers [53], cyclodextrins [54, 55], proteins such as bacteriorhodopsin [56], and 3D polycyclics such as cubane [57] and adamantane [58]. Typically, azo chromophores are embedded in a solid matrix for studies and devices. As a result, matrix effects are inescapable: the behavior of the chromophore is altered due to the matrix, and in turn the chromophore alters the matrix [59]. Although either could be viewed as a nuisance, both are in fact useful: the chromophore can be used as a probe of the matrix (free volume, polarizability, mobility, etc.), and when the matrix couples to chromophore motion, molecular motions can be translated to larger lengthscales. Thus, the incorporation strategy is critical to exploiting azobenzene's unique behavior.

2.3.1. Thin Polymer Films

Doping azobenzenes into polymer matrices is a convenient inclusion technique [60, 61]. These “guest–host” systems can be cast or spin-coated from solution mixtures of polymer and azo small molecules, where the azo content in the thin film is easily adjusted via concentration. Although doping leaves the azo chromophores free to undergo photoinduced motion unhindered, it has been found that many interesting photomechanical effects do not couple to the matrix in these systems. Furthermore, the azo mobility often leads to instabilities, such as phase-separation or microcrystallization. Thus, one of the most attractive methodologies for incorporating azobenzene into functional materials is by covalent attachment to polymers. The resulting materials benefit from the inherent stability, rigidity, and processability of polymers, in addition to the unusual photoresponsive behavior of the azo moieties. Both side-chain and main-chain azobenzene polymers have been prepared [62] (Fig. 5). Reported synthetic strategies involve either polymerizing azobenzene-functionalized monomers [63, 64] or post-functionalizing a polymer that has an appropriate pendant group (usually a phenyl) [65–67]. The first method is preferred for its simplicity and control of sequence distribution. The second takes advantage of commonly available starting materials but may require more reaction steps. Many different backbones have been used as scaffolds for azo moieties, including imides [68], esters [69], urethanes [70], ethers [71], organometallic ferrocene polymers [72], dendrimers [73, 74], and even conjugated polydiacetylenes [75], polyacetylenes [76], and main-chain azobenzenes [77, 78]. The most common azo-polymers are acrylates [79], methacrylates [80], and isocyanates [81]. Thin films are usually prepared by spin-coating [82–85], although there are also many examples of using solvent evaporation, the Langmuir–Blodgett technique [86–89], and self-assembled monolayers [90]. Spin-cast films are typically annealed above the polymer glass-transition temperature (T_g) to remove residual solvent and erase any hydrodynamically induced anisotropy.

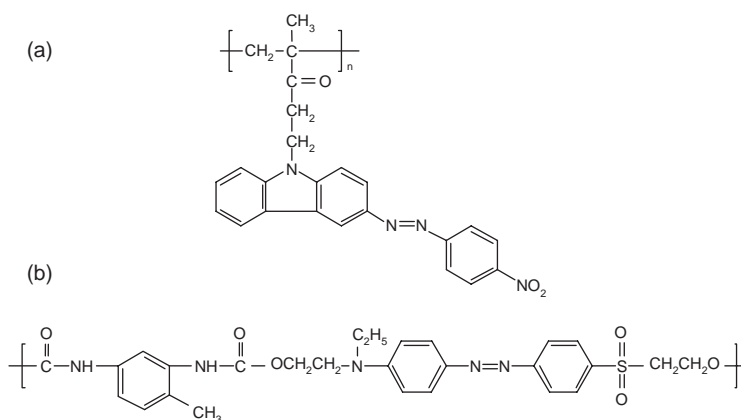


Figure 5. Examples of azo-polymer structures, showing that both (a) side-chain and (b) main-chain architectures are possible [64, 210].

2.3.2. Liquid Crystals

Azobenzenes are anisotropic, rigid molecules and as such are ideal candidates to act as mesogens: molecules that form liquid-crystalline (LC) mesophases. Many examples of small-molecule azobenzene liquid crystals have been studied. Some azo-polymers also form LC phases (refer to Fig. 6 for a typical structure). For side-chain azobenzenes, a certain amount of mobility is required for LC phases to be present; as a rule, if the tether between the chromophore and the backbone is less than six alkyl units long, the polymer will exhibit an amorphous and isotropic solid-state phase, whereas if the spacer is longer, LC phases typically form. The photoisomerization of azobenzene leads to modification of the phase and alignment (director) in LC systems [59, 91]. The director of a liquid crystal phase can be modified by orienting chromophores doped into the phase [92, 93], by using an azobenzene-modified “command surface” [94–96], using azo copolymers [97], and, of course, in pure azobenzene LC phases [98, 99]. One can force the LC phase to adopt an in-plane order (director parallel to surface), homeotropic alignment (director perpendicular to surface), or tilted or even biaxial orientation [100]. These changes are fast and reversible. While the *trans* azobenzenes are excellent mesogens, the *cis* azos typically are not. If even a small number of azo molecules are distributed in an LC phase, *trans* → *cis* isomerization can destabilize the phase by lowering the nematic-to-isotropic phase transition temperature [101]. This enables fast isothermal photocontrol of phase transitions [36, 102–104]. Since these modulations are photoinitiated, it is straightforward to create patterns [105]. These LC photoswitching effects are obviously attractive in many applications, such as for display devices, optical memories [94], electro-optics [106], modulation of the polarization of ferroelectric liquid crystals [107, 108], etc.

2.3.3. Dendrimers

Dendrimers have been investigated as unique structures to exploit and harness azobenzene’s photochemistry [109–111]. Dendrimers with strongly absorbing pendants can act as antennae: harvesting light and making it available, via intramolecular energy transfer, to the dendrimer core. In dendrimers with azo cores, this allows for the activation of isomerization using a wavelength outside of the azo absorption band (since the dendrimer arms absorb

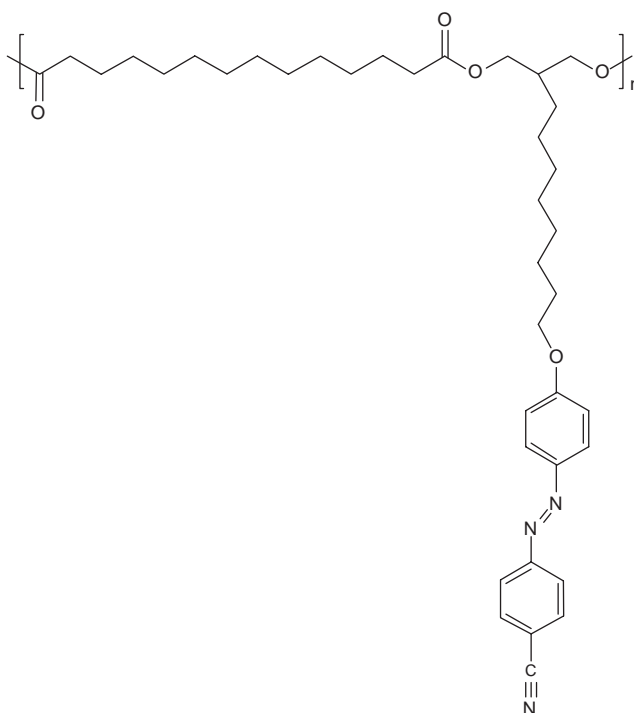


Figure 6. A typical liquid-crystalline side-chain azobenzene polymer [99].

and transfer energy to the core) [112, 113]. Furthermore the configurational change that results from the core isomerization will translate into a larger scale geometric change. For instance, in a dendrimer with three azobenzene arms (Fig. 7), the various isomerization combinations (EEE, EEZ, EZZ, and ZZZ) could all be separated by thin-layer chromatography due to their different physical properties [114]. The conformational change associated with isomerization modifies (typically reduces) the hydrodynamic volume, with the specific extent of conformational change depending strongly on where the azo units are incorporated [115].

2.3.4. Polyelectrolyte Multilayers

A new facile and versatile film preparation technique, layer-by-layer electrostatic self-assembly, has become the subject of intensive research since its introduction by Decher [116–119]. In this technique, a charged or hydrophilic substrate is immersed in a solution of charged polymers (polyelectrolytes), which adsorb irreversibly onto the substrate. After rinsing, the substrate is then immersed in a solution containing a polyelectrolyte of opposite charge, which adsorbs electrostatically to the charged polymer monolayer. Because each layer of adsorbed polymer reverses the surface charge, one can build up an arbitrary number of alternating polycation–polyanion layers. These polyelectrolyte multilayers (PEMs) are easy to prepare, use benign (all-aqueous) chemistry, and are inherently tunable [120–122]. Specifically, by adjusting the ionic strength [123–126] or pH [127–130] (in the case of “weak” polyelectrolytes) of the assembly solution, the polyelectrolyte chain conformation is modified,

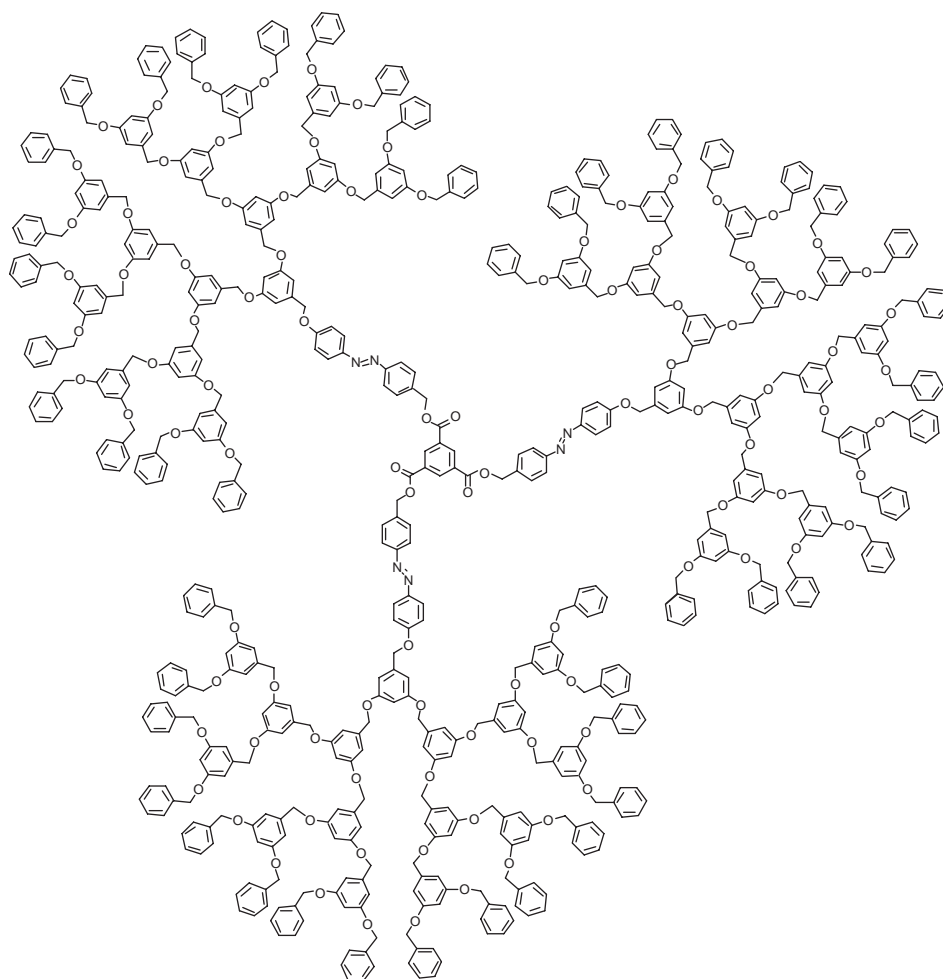


Figure 7. An azobenzene dendrimer containing three azo moieties [114]. Each chromophore has two isomerization states (*trans* and *cis*), leading to four distinct photo-isomers for the dendrimer molecule. All four isomers have different physical properties.

and hence the resulting film architecture is tuned. For instance, one can control thickness [124, 131], permeability [132], morphology [133–135], and density [136]. Recently, the technique has been modified to assemble the alternate layers using a spin-coater, which reduces the assembly times and adsorption solution volumes considerably [137–140].

As a film preparation technique, this method has numerous advantages. The adsorption of the polymers is quasi-thermodynamic, with the chains adsorbing into a local minimum, which makes the films stable against many defects (dewetting, pinhole formation, etc.). Importantly, the technique is not limited to flat surfaces: any geometry that can be immersed in solution (or have solution flowed-through) is suitable. Colloids have been efficiently coated with PEMs [141, 142], and by dissolving the core one can also form hollow PEM microcapsules [143]. Multilayers can be formed on nearly any material (glass, quartz, silicon, most metals, etc.) and are robust against thermal and solvent treatment [144]. One of the main interests in PEMs is due to their inherent biocompatibility [145]: multilayers have been formed on enzyme microcrystals [146], used to encapsulate living cells [147], and used to coat arterial walls [148]. Perhaps the most useful feature of the multilayering technique is its ability to incorporate secondary functional groups into the thin film structure. The location of these functional units (which may be small molecules, pendants on the polyelectrolyte chains, or particles) within the multilayer stack can be controlled with subnanometer precision. A wide variety of functionalities have been demonstrated, including organic molecules [149], synthetic polymers [150], biopolymers [151], natural proteins [152], colloids [153], inorganic nanoparticles [154], clay platelets [155] (used as a nacre biomimic [156]), dendrimers [157], electrochemically active species [120], functionalized C_{60} [158], and even, counter-intuitively, uncharged and nonpolar polymer chains [159].

Many research groups have investigated the possibility of incorporating optically responsive azobenzene chromophores into the versatile PEM structures (examples presented in Fig. 8), including Advincula [160–163], Kumar and Tripathy [150, 164], Tieke [165–168], Heflin [169], and Barrett [170, 171]. In some cases, copolymers are synthesized, where some of the repeat units are charged groups and some are azo chromophores [172, 173]. These materials may, however, have solubility issues, as the azo chromophore is typically not water soluble. Efforts have therefore gone into synthesizing azo-ions [174, 175], or polymers where the charge appears on the azobenzene unit [173, 176, 177]. The azobenzene chromophore may also be created by post-functionalization of an assembled PEM [164]. Azobenzene-functionalized PEMs have demonstrated all of the unique photophysics associated with the chromophore, including induced birefringence [162, 178] and surface mass transport [176] (which will be described in more detail in Section 4). It should be noted, however, that in general the quality of the patterning is lower [177], presumably due to the constraints to chain motion that the ionic “cross-links” engender. There are many examples of performing the multilayering with a polyelectrolyte and a small molecule azobenzene ionic dye [136]. In contrast to conventional doped systems, the chromophores in these systems do

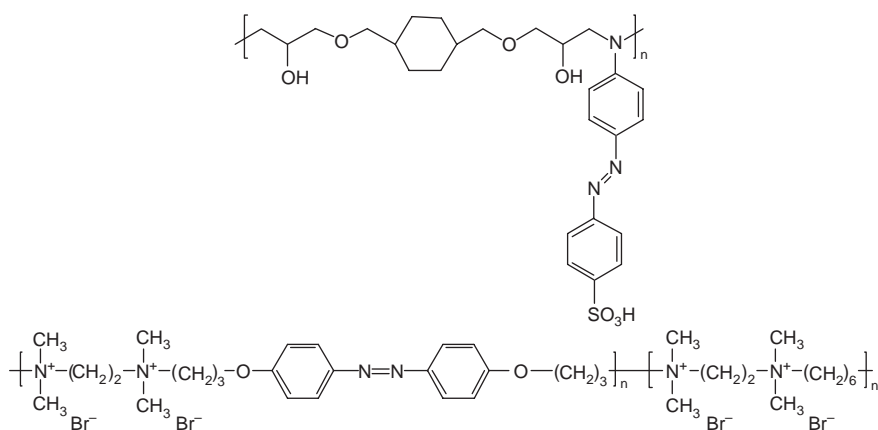


Figure 8. Examples of water-soluble azo-polyelectrolytes, which can be used in the preparation of photoactive polyelectrolyte multilayers [150, 167].

not suffer from aggregation instabilities [160], and the azo photomotions do couple to the matrix, as evidenced by birefringence [179, 180] and surface patterning [149, 181]. These effects can again be attributed to the fact that the ionic attachment points act as cross-links in a dry PEM sample. The aggregation and photochemical behavior of the azo chromophore (absorbance spectrum, isomerization rate, etc.) vary depending on the nature of the counter-polymer [182] (and, of course, is affected by any ionic ring substituent). These may be viewed as undesirable matrix effects, or as a way to tune the chromophore response. The multilayering technique does not offer the precision and reproducibility of conventional inorganic film preparation techniques. It is, however, simple and versatile and offers the possibility of combining unique structures and functionalities (for instance, it has been used to create superhydrophobic surfaces [183] and to make azo-photochromic hollow shells [175] and is amenable to patterning [184]). While it is unlikely to replace established techniques for high-performance devices, it may find applications in certain niches (coatings, disposable electronics, biomedical devices, etc.).

3. PHOTOINDUCED MOTIONS AND MODULATIONS

Irradiation with light produces molecular changes in azobenzenes, and under appropriate conditions, these changes can translate into larger scale motions and even modulation of material properties. Following Natansohn and Rochon [185], we will describe motions roughly in order of increasing size scale. However, since the motion on any size scale invariably affects (and is affected by) other scales, clear divisions are not possible. In all cases, some of the implicated applications, photoswitching, and photomodulations will be outlined.

3.1. Molecular Motion

The fundamental molecular photo-motion in azobenzenes is the geometrical change that occurs upon absorption of light. In *cis*-azobenzene, the phenyl rings are twisted at 90° relative to the C—N=N—C plane [28, 186]. Isomerization reduces the distance between the 4- and 4'-positions from 0.99 nm in the *trans* state to 0.55 nm for the *cis* state [187–189]. This geometric change increases the dipole moment: whereas the *trans* form has no dipole moment, the *cis* form has a dipole moment of 3.1 D [17]. The free volume requirement of the *cis* is larger than that of the *trans* [190], and it has been estimated that the minimum free volume pocket required to allow isomerization to proceed via the inversion pathway [28, 38] is 0.12 nm^3 , and via the rotation pathway [13] it is approximately 0.38 nm^3 . The effects of matrix free volume constraints on photochemical reactions in general have been considered [191]. The geometrical changes in azobenzene are very large, by molecular standards, and it is thus no surprise that isomerization modifies a wide host of material properties.

This molecular displacement generates a nanoscale force, which has been measured in single-molecule force spectroscopy experiments [192, 193]. In these experiments, illumination causes contraction of an azobenzene polymer, showing that each chromophore can exert pN molecular forces on demand. A pseudo-rotaxane that can be reversibly threaded–dethreaded using light has been called an “artificial molecular-level machine” [194, 195]. The ability to activate and power molecular-level devices using light is of course attractive, since it circumvents the limitations inherent to diffusion or wiring. The fast response and lack of waste products in azo isomerization are also advantageous. Coupling these molecular-scale motions to do useful work is of course the next challenging step. Progress in this direction is evident from a wide variety of molecular switches that have been synthesized. For example, an azo linking two porphyrin rings enabled photocontrol of electron transfer [196]. In another example, dramatically different hydrogen-bonding networks (intermolecular and intramolecular) can be favored based on the isomeric state of the azo group linking two cyclic peptides [197, 198].

3.2. Photo Orientation

Azobenzene chromophores can be oriented using polarized light, via a statistical selection process, described schematically in Figure 9. Azobenzenes preferentially absorb light

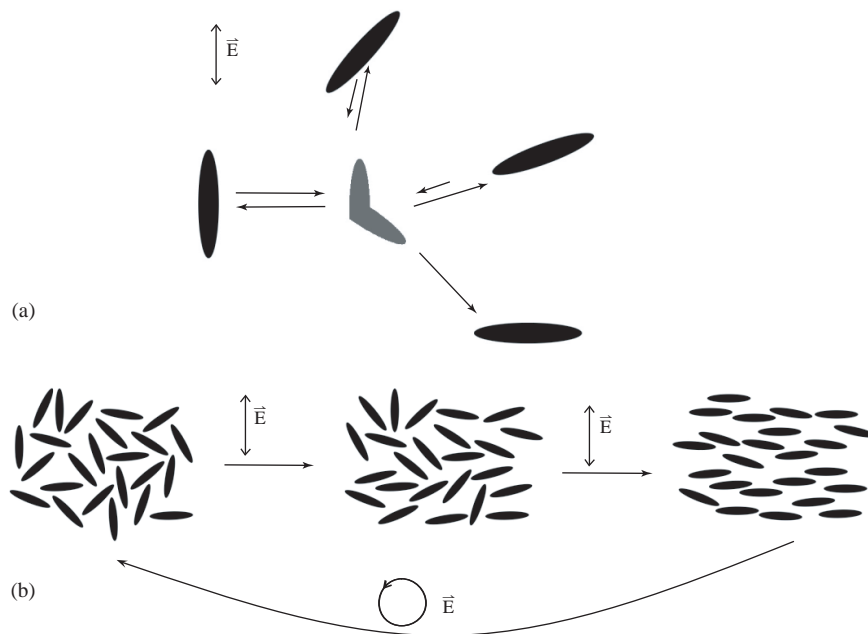


Figure 9. Statistical photo-orientation of azo molecules. (a) The molecules aligned along the polarization direction of the incident light absorb, isomerize, and re-orient. Those aligned perpendicular cannot absorb and remain fixed. (b) Irradiation of an isotropic samples leads to accumulation of chromophores in the perpendicular direction. Circularly polarized light restores isotropy.

polarized along their transition dipole axis (long axis of the azo molecule). The probability of absorption varies as $\cos^2 \phi$, where ϕ is the angle between the light polarization and the azo dipole axis. Thus, azos oriented along the polarization of the light will absorb, whereas those oriented against the light polarization will not. For a given initial angular distribution of chromophores, many will absorb, convert into the cis form, and then revert to the trans form with a new random direction. Those chromophores that fall perpendicular to the light polarization will no longer isomerize and reorient; hence, there is a net depletion of chromophores aligned with the light polarization, with a concomitant increase in the population of chromophores aligned perpendicular (i.e., orientation hole burning). This statistical reorientation is fast, and gives rise to strong birefringence (anisotropy in refractive index) and dichroism (anisotropy in absorption spectrum) due to the large anisotropy of the azo electronic system. The process is especially efficient due to the mesogenlike cooperative motion that the azobenzene groups facilitate, even in amorphous samples below T_g [97]. Since the process requires cycling of the chromophores between trans and cis states, the pseudo-stilbenes have the fastest response.

The orientation due to polarized light is reversible. The direction can be modified by using a new polarization direction for the irradiating light. Circularly polarized light will randomize the chromophore orientations. It must be emphasized, however, that there is another preferential alignment direction during irradiation: along the axis of the incoming light. It is unavoidable that chromophores will efficiently build-up aligned along the irradiation axis, but this is often ignored in the literature or characterized as “photobleaching” when in fact it is a reversible photoalignment (albeit one that reduces the absorbance as viewed by any photoprobe). Because unpolarized light can photo-orient (along the axis of illumination) [85], even sunlight is suitable. The motion of the sun through the sky over the course of a day can cause orientation at different tilt angles [199]. This causes chromophores at different depths to be oriented in different directions, which produces a net chiral helical ordering in the film of a particular handedness (based on the hemisphere in which the experiment is performed). The implications of such results to the origin of absolute chirality in biological systems are intriguing.

3.2.1. Birefringence

Irradiation with light polarized in the y -direction will lead to net alignment of chromophores in the x -direction. As a result, the refractive index probed in the x -direction, n_x , will measure the azo long axis and will be larger than n_y . Birefringence is the anisotropy in refractive index: $\Delta n = n_x - n_y$. Photoalignment in azobenzene systems can achieve extremely high values of Δn , up to 0.3–0.5 at ~ 633 nm [200, 201]. Importantly, very high birefringence values can be obtained far outside of the azo absorption band, which means that the birefringence can be utilized/measured without disturbing the chromophores. An in-plane isotropic state ($n_x = n_y$) can be restored by irradiation with circularly polarized light, and a fully isotropic state can be obtained by heating above the glass-transition temperature.

The exact nature of the orientation can be rigorously quantified using optical techniques. Using surface plasmon resonance spectroscopy or waveguide spectroscopy, the three orthogonal refractive indices in an oriented sample can be measured [202]. Stokes polarimetry can be used to fully characterize the optical anisotropy, separating linear and circular components [203]. The anisotropy of the *cis* population during irradiation can also be measured in some systems [204, 205], where it is found that, as with *trans*, there is an enrichment perpendicular to the irradiation polarization. In some LC systems, however, the *cis* population may preferentially align with the irradiating polarization (which may be attributed to an optical Fréedericksz transition) [206].

The birefringence can be written and erased hundreds of thousands of times, which is important technologically [207]. Amorphous polymer systems with relatively high glass-transition temperatures exhibit good temporal stability of any induced orientation. Upon heating, some order will be lost, with full isotropy restored after heating past T_g . A short spacer between the chromophore and the polymer backbone slows the growth of birefringence yet promotes stability, owing to hindered motion. Surprisingly, main-chain azos can achieve high levels of birefringence, indicating relatively high polymer mobility [208–210]. As might be expected, (nanosecond) pulsed experiments lead to thermal effects, which enhance chromophore motion, and thereby induced greater birefringence, at the same net dose, compared to continuous-wave (cw) experiments [211, 212]. At very high pulsed fluence, the thermal effects were too great and erased the induced birefringence.

The easily inscribed and erased birefringence has a number of unique applications. Most readily, it can be used to create wave-plates [213] and polarization filters, which can be used to separate right-handed from left-handed circularly polarized light [214]. The strong refractive index contrast, if patterned into a line, can serve as a channel waveguide [215, 216]. This offers the unique possibility of optical devices that can be patterned, erased, and reused. In principle, these photonic circuits could be altered during device operation, enabling optical routing of optical signals (i.e., optical computing). The switching of orientational order can thus be used as an all-optical switch [217]. By illuminating an azo sample with a spatially varying light pattern, birefringence gratings can also be formed [218–220]. These are phase gratings, as opposed to amplitude gratings, and diffract light based on spatial variation of the refractive index. This is the essence of holography: two interfering coherent beams generate a spatially varying light pattern, which is encoded into the material. Under illumination of the material with one of the beams, the diffraction reproduces the other encoded beam. In the case of liquid crystal samples, light induces a spatial pattern of nematic and isotropic zones (which have different refractive indices). These holographic phase grating can be rapidly formed, erased, and switched [221].

3.2.2. Nonlinear Optics

The requirements for nonlinear optical (NLO) response in any material is an asymmetric (strictly, anharmonic) response of the electronic system. Pseudo-stilbenes, which have push/pull substituents, have a strongly asymmetric electron distribution, which makes them ideal NLO molecules (see, for instance, Fig. 10). For a bulk NLO response, one requires an overall noncentrosymmetric material. This requirement is achieved in many inorganic crystals. In organic systems, the broken symmetry is typically obtained by applying an electric field at a temperature sufficient to allow for the molecular dipoles to align with the field.

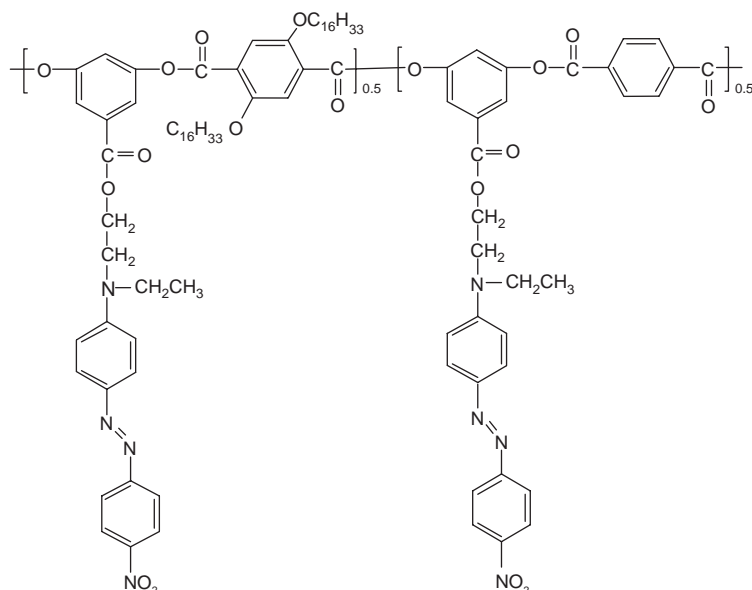


Figure 10. Example of a non-linear optic azo-polymer, used for photo-assisted poling [230].

This process is called electric field poling and is accomplished using interdigitated or flat electrodes or a sharp charged needle (or grid) held above a grounded sample (called corona poling). The NLO response is typically quantified using second-harmonic generation (SHG; the emission of light at double the frequency of the incident beam), the electrooptic effect (change of refractive index upon application of an electric field), or wave mixing experiments (where various frequencies of light can be synthesized or enhanced). These also constitute the main applications of NLO materials: they can be used to synthesize new frequencies of light, to electrically switch a beam, or to allow two beams of light to interact and couple (which can form the basis of an all-optical switch) [222].

Azo-polymers have been shown to be excellent NLO materials [7, 223–225]. In azo systems, one has the additional advantage of using light to affect the chromophores. Although photoalignment orients the chromophore axis, it does not select out a preferred direction for the molecular dipole (thus, an equal number of dipoles point “left” and point “right”). In fact, evidence suggests that dipoles in these systems tend to orient antiparallel (H-aggregates) [226, 227], thereby canceling polar order. Nevertheless, the photoalignment can be used to facilitate the electric poling, enabling it to be performed at room temperature and with a small dc field [228–231]. Furthermore, by using polarized light and its harmonic, a net non-centrosymmetry can be obtained in an all-optical process [232, 233]. This occurs because the mixture of a primary beam and its second harmonic creates a directional electric field in the material.

Another interesting approach for NLO uses dendrons (“half-dendrimers”) with azo functionalities [234]. The dendritic architecture forces all the chromophores within the dendron to align, which strongly enhances the NLO response. The dendron had a first-order molecular hyperpolarizability 20 times larger than the monomer. With regard to applications, the azos have been shown to function as electro-optical switches [235] and to exhibit photorefraction [64, 236–238], an NLO effect where photoconductivity permits light to establish a space charge grating, whose associated index grating refracts a probe light beam.

3.3. Domain Motion

The orientation and reorientation of liquid-crystalline domains has already been outlined. The azo chromophores act as mesogens, and their photoalignment becomes transferred to the LC host. A very small azo content (a few mole percent [102]) can lead to orientational control of LC domains. This is an excellent example of amplification of the azo molecular motion. The phase of a liquid crystal can also be switched with light. Irradiation produces

cis isomers, which are poor mesogens and destabilize the nematic phase, thereby inducing a phase transition to the isotropic state. There are comparatively few examples of phototrigged increases in LC ordering. In one case, a nanoscale phase separation of the cis isomers led to a net increase in the order parameter of the LC phase [239]. In another system, a chiral azo was found to induce a cholesteric phase when it was in the cis state [240].

With liquid-crystalline [241] or preoriented amorphous samples [242], one can photoinduce a chiral domain structure. Incident circularly polarized light becomes elliptically polarized due to the first oriented layer. This ellipse subsequently reorients deeper chromophores, which in turn modify the ellipticity of the light. This reorientation continues throughout the film depth. Overall, a chiral ordering of the chromophore domains is established [243]. Remarkably, one can switch between a right- and left-handed supramolecular helix at will, by changing the incident light handedness. There are many other examples of photocontrol of supramolecular order. The pitch of a cholesteric LC can be modified by isomerization [244]. Biomacromolecular variants abound [51]. Azo-modified polypeptides can be photoswitched between ordered states (α -helix or β -sheet) and a random coil [245–247]. The duplex of modified DNA can be reversibly switched [248], and the catalytic activity of histidine can be controlled [249].

Photoisomerization can also affect self-assembly behavior at the domain level. On irradiation, one can induce a phase change [250], a solubility change [251, 252], crystallization [253], or even reversal of phase separation [254]. The critical micelle concentration (cmc) and surface activity can also be modified [255]. In an amphiphilic polypeptide system, self-assembled micelles were formed in the dark and could be disaggregated with light [256]. When allowed to assemble as a transmembrane structure, the aggregate could be reversibly formed and destroyed with light, which allowed for reversible photoswitching of ion transport [257]. Related experiments on methacrylates [258, 259] and polypeptides [260] showed that a polymer's chiral helix could be reversibly suppressed on irradiation. In a series of polyisocyanate polymers, it could be selected whether irradiation would suppress or increase chirality [261, 262].

3.4. Micrometer-Scale Motion

The azos exhibit a unique and remarkable surface-mass transport under light illumination. This optical patterning represents massive material transport on a micrometer and submicrometer length scale. This mass transport provides a unique opportunity for nanostructure formation and will be described in detail in Section 4.

3.5. Macroscopic Motion

It is interesting to study whether the azobenzene molecular conformational changes can result in changes to bulk phenomena or even to macroscopic motion. The first consideration is whether the material expands to an appreciable extent. In monolayers, it is well established that the larger molecular size of the cis leads to a corresponding lateral expansion [263], which can modify other bulk properties. For instance, this allows photomodulation of a monolayer's water contact angle [264] or surface potential [265]. Using fluorinated azo-polymer, good photocontrol [266] and photopatterning [267] of wettability has been demonstrated. A monolayer of azo-modified calixarene, when irradiated with a light gradient, produced a gradient in surface energy sufficient to move a macroscopic oil droplet [268], suggesting possible applications in microfluidics. Modest photoinduced contact angle changes for thin polymer films have also been reported [41].

In layered inorganic systems with intercalated azobenzenes, reversible photochanges in the basal spacing (on the order of 4%) can be achieved [269, 270]. In polymer films, there is some evidence that the film thickness increases, as measured by ellipsometry [215] (the refractive index certainly changes [271], but this is not an unambiguous demonstration of expansion/contraction). Related are experiments that show that external applied pressure tends to hinder photoisomerization [272]. Photocontraction for semicrystalline main-chain azos has been measured [68, 273]. This photomechanical response presumably occurs because of the shortening of the polymer chains upon trans \rightarrow cis conversion. On the other hand,

photoexpansion would seem to be contradicted by positron lifetime experiments that suggest no change in microscopic free volume cavity size during irradiation [274]. More conclusive experiments are in order.

The most convincing demonstration of macroscopic motion due to azo isomerization is the mechanical bending and unbending of a free-standing polymer film [275, 276]. The macroscopic bending direction may be selected either with polarized light or by aligning the chromophores with rubbing. Bending occurs in these relatively thick films because the free surface (which absorbs light) contracts, whereas the interior of the film (which is not irradiated owing to the strong absorption of the upper part of the film) does not contract. That these materials contract (rather than expand) appears again to be related to the main-chain azo groups and may also be related to the LC nature of the cross-linked gels. For a thin film floating on a water surface, a contraction in the direction of polarized light was seen for LC materials, whereas an expansion was seen for amorphous materials [277]. A related amplification of azo motion to macroscopic motion is the photoinduced bending of a microcantilever coated with an azobenzene monolayer [278]. One can also invert the coupling of mechanical and optical effects: by stretching an elastomeric azo film containing a grating, one can affect its wavelength-selection properties and orient chromophores [279].

3.6. Other Applications of Azobenzenes

3.6.1. Photoswitches

As already pointed out, azo isomerization can be used to photoswitch a wide variety of other properties (at numerous size scales). In addition to the optical changes already described, it is worth noting that the transient change in material refractive index (due to the different n of cis and trans) can itself act as a photoswitch [280]. The azo photochromism has even been suggested as a possible optical neural network element [281]. Binding and transport properties can also be photoswitched [83, 282]. In some systems the redox potential and ionic conductivity can be switched with light [283]. Crown ethers [284, 285] and calixarenes [286] functionalized with azobenzene can be used as reversible ion-binding systems. Thus, ion transport can be photoregulated. In other cases, the transport properties can be photocontrolled not via binding, but based on changes in pore sizes [287–289]. In a particularly elegant example, the size of nanochannels could be modified by irradiating azo ligands which decorated the channel walls [290]. Azo-derivatized gramicidin ion channels represent a unique case where ion transport can be photocontrolled by optical manipulation of a biomolecule [291]. In addition to obvious applications in controlled transport, this offers the possibility of studying cells by controlling the timing of the ion exchange processes. Photoinduced catalysis is also possible: for instance, using molecules where only the cis form is catalytically active [292]. Extension of the molecular imprinting technique to azo-polymers allows for photoswitching of binding activity with respect to the imprinted molecule [293].

3.6.2. Photoprobes

The properties of an azo chromophore (spectrum, isomerization kinetics, etc.) depend strongly on the local environment. This enables the possibility of using the chromophore as a molecular sensing element: a photoprobe. For instance, it has been found that many azo properties depend on local H^+ concentration, to the extent that the azo can in fact be used as a pH meter [144, 294]. As already mentioned, the isomerization kinetics can also be used as a probe of free volume [13, 190], local aggregation [42], or phase transitions. The azo molecule is small and exhibits clean photochemistry, which makes it more versatile and robust than many other photoprobes. The rate of isomerization is also remarkably insensitive to temperature [295]. This is an area of research that deserves considerably more attention.

In a more sophisticated example, azo chromophores were used to monitor protein folding [296, 297]. Specifically, femtosecond two-dimensional infrared (2D IR) spectroscopy was used to monitor the distances between carbonyl groups in the peptide. An azo chromophore, incorporated inside the polypeptide chain, was used as a photoswitch to initiate a conformational change, hence initiate protein folding, on demand. Combined with time-resolved

monitoring of the azo spectrum, this allows the deconvolution of folding dynamics. Pump-probe ultrafast laser pulse experiments are being used to study many different chemical reactions but are obviously limited to reactions that can be triggered by light. Incorporating azobenzene into the experiment allows a wider range of reactions to be phototriggered.

3.6.3. Optical Data Storage

The azos have been investigated as optical storage media for some time. Early proofs of principle were on Langmuir-Blodgett films, using photochromism [298] or birefringence [299]. Increasingly, amorphous polymer systems are being recognized as promising materials. In these easily processed systems, the birefringence is strong, stable, and switchable, making them ideal for optical memories. A single domain could encode one bit by either being isotropic or birefringent, a difference that is easily probed optically. The Δn values are large enough, in fact, that a gray-level algorithm could be used, where each domain stores more than one bit of data. On the negative side, the photoalignment generated in the direction of the read/write beam leads to an effective loss of material performance with time. Full anisotropy could be restored with heat, however (which can be local and photoinduced, with appropriate device setup). The feasibility of storing ~ 30 Gbytes of data on a single-layer of a removable disk using this gray-level approach has been demonstrated [201].

Even the fastest photoinduced birefringence in azo systems requires milliseconds and is slow compared to most computer timescales. However, optical data storage is amenable to gray-level read/write [300] and to storing/retrieving full two-dimensional "pages" of data at a time. In principle, azo systems could achieve high data storage and retrieval speeds. The full three-dimensional volume of a material can be used by encoding many layers of two-dimensional data (pages) one on top of the other [301, 302]. This is accomplished by moving the optical focal plane through the material.

An intriguing possibility for high-density storage is to use angular multiplexing [201]. By storing multiple superimposed holograms in a single material, the data density is increased dramatically, and the whole three-dimensional volume of the material is exploited [303]. Volume phase holograms in azo systems can have diffraction efficiencies greater than 90% [304], making data readout robust. The hologram is encoded by interfering a reference beam and a writing beam inside the sample volume, at a particular angle. The write beam, having passed through a spatial light modulator (SLM), has a pattern corresponding to the data, which is then holographically encoded in the sample. The entire page of data is written at once. By selecting different angles, new pages of data can be written. To readout a page, the azo-sample is set at the correct angle and illuminated with the reference beam. The resulting diffraction pattern is imaged on a CCD array, which measures the encoded beam pattern (data). The volume of data and transmission rate is clearly large: projections of ~ 1000 Gbytes in a single disk have been made. Since the entire hologram image is stored throughout the material, the technique is fairly insensitive to dust, scratches, and pinpoint defects.

The use of azo-substituted peptide oligomers appears to enable control of the order, hence optimization for holographic applications [305]. Optical memories would be considerably enhanced by using two-photon processes. This allows the addressable volume to be smaller and better defined, while reducing cross-talk between encoded pages. Some azo chromophores exhibit "biphotonic" phenomena, which could be employed to enhance optical data storage.

4. SURFACE MASS TRANSPORT

In 1995, a surprising and unprecedented optical effect was discovered in polymer thin films containing the azo chromophore Disperse Red 1 (DR1), shown in Figure 11. The Natansohn/Rochon [306] research team and the Tripathy/Kumar collaboration [307] simultaneously and independently discovered a large-scale surface mass transport when the films were irradiated with a light interference pattern. In a typical experiment, two coherent laser beams, with a wavelength in the azo absorption band, are intersected at the sample surface (refer to Fig. 12). The sample usually consists of a thin spin-cast film (10–1000 nm)

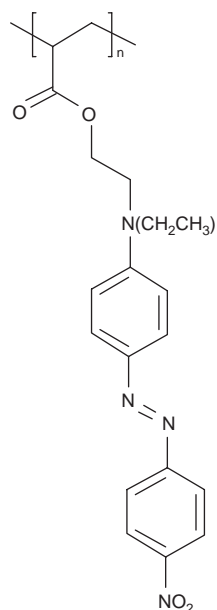


Figure 11. Chemical structure of poly(disperse red 1) acrylate, pDR1A, a pseudo-stilbene side-chain azo-polymer that generates high-quality surface-relief structures.

of an amorphous azo-polymer on a transparent substrate. The sinusoidal light interference pattern at the sample surface leads to a sinusoidal surface patterning, i.e., a surface relief grating (SRG). These gratings were found to be extremely large, up to hundreds of nanometers, as confirmed by AFM (Fig. 13). The SRGs diffract very efficiently, and in retrospect it is clear that many reports of large diffraction efficiency prior to 1995, attributed to birefringence, were in fact due to surface gratings. The process occurs readily at room temperature (well below the T_g of the amorphous polymers used) with moderate irradiation ($1\text{--}100\text{ mW/cm}^2$) over seconds to minutes. The phenomenon is a reversible mass transport, not irreversible material ablation, since a flat film with the original thickness is recovered upon heating above T_g . Critically, it requires the presence and isomerization of azobenzene

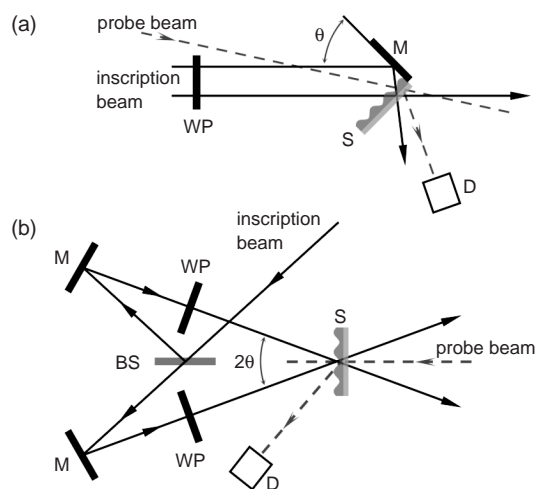


Figure 12. Experimental setup for the inscription of a surface relief grating: S refers to the sample, M are mirrors, D is a detector for the diffraction of the probe beam, WP is a waveplate (or generally a combination of polarizing elements), and BS is a 50% beam splitter. The probe beam is usually a HeNe (633 nm) and the inscription beam is chosen based on the chromophore absorption band (often Ar^+ 488 nm). (a) A simple one-beam inscription involves reflecting half of the incident beam off of a mirror adjacent to the sample. (b) A two-beam interference setup enables independent manipulation of the polarization state of the two incident beams.

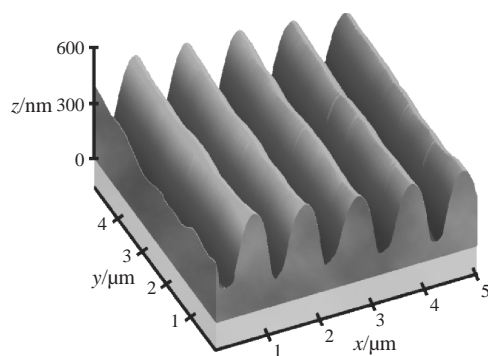


Figure 13. AFM image of a typical surface relief grating (SRG) optically inscribed into an azo-polymer film. Grating amplitudes of hundreds of nanometers, on the order of the original film thickness, are easily obtained. In this image, the approximate location of the film-substrate interface has been set to $z = 0$, based on knowledge of the film thickness.

chromophores. Other absorbing but nonisomerizing chromophores do not produce SRGs. Many other systems can exhibit optical surface patterning [308], but the amplitude of the modification is much smaller, does not involve mass transport, and usually requires additional processing steps. The all-optical patterning unique to azobenzenes has been studied intensively since its discovery, yet there remains controversy regarding the mechanism. The competing interpretations will be discussed and evaluated here. Many reviews of the remarkable body of experimental results are available [7, 62, 185, 309].

4.1. Experimental Observations

4.1.1. Dependence on Optical Parameters

The surface mass patterning unique to azobenzenes is a fundamentally optical process, whereby the incident light pattern is encoded in the material. In a surface relief grating experiment, two beams are intersected at an angle 2θ at the sample surface, giving rise to an SRG with period:

$$\Lambda = \frac{\lambda}{2 \sin \theta} \quad (1)$$

where λ is the wavelength of the inscription light. The amplitude (height) of the SRG depends upon the inscription angle, displaying a maximum at $\theta \sim 15^\circ$ [310, 311]. Grating height increases nonlinearly with irradiation time and power, up to a saturation point [312, 313]. At moderate fluence, the grating efficiency depends only on the net exposure, not on the temporal distribution of irradiation. Gratings can be formed with intensities as low as 1 mW/cm^2 , as long as the inscription wavelength is within the azo absorption band. Most chromophores used for SRG formation have a strong overlap of their *trans* and *cis* absorption spectra, allowing both isomers to be excited with a single wavelength. On the other hand, some experiments have been performed using azobenzenes with *trans* absorption in the blue, and *cis* absorption in the red [314, 315]. Using an interference pattern of red HeNe beams, inscription only occurs if a blue pump beam concurrently irradiates. This biphotonic phenomenon proves that cycling of chromophores, and not simply isomerization, is required for grating formation.

The phase relationship between the incident light field and the resulting surface deformation is crucial in understanding the mechanism of grating formation (Fig. 14). Early investigations using the diffraction of an edge [306, 316, 317] and single-beam surface deformations [318] convincingly showed that the light and surface relief are 180° out of phase. That is, light intensity maxima correspond to valleys in the surface relief. In effect, material is moved out of the light and into the dark regions. This rule appears to hold in the majority of cases, yet in a number of systems the phase relationship seems to be exactly inverted, with mass transport into illuminated regions. Specifically, in certain liquid-crystalline systems, the phase behavior is inverted [277, 319, 320]. In one study, an amorphous material exhibited the “usual” phase

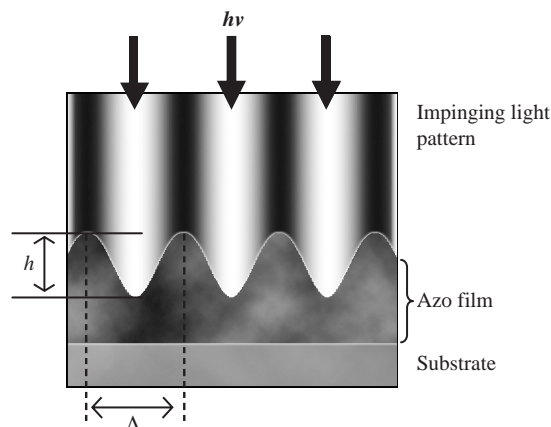


Figure 14. Schematic of a grating with spacing Λ and amplitude h . The usual phase relationship is indicated: light intensity maxima correspond to valleys in the surface relief.

behavior, and a thin film of this polymer floating on water expanded in the direction of the light polarization. A similar LC azo-polymer exhibited inverted phase behavior in SRG experiments, and contracted in the direction of polarized illumination as a floating film. The tempting conclusion is that amorphous and polymeric systems exhibit opposite photomechanical response, which translates into opposite phase behavior in grating inscription. A possibly relevant experiment showed that for LC systems, the *cis* chromophores may become preferentially oriented along the light polarization direction, instead of perpendicular to it [206]. It should be pointed out, however, that some LC systems exhibit the “usual” phase relationship [321], and in one LC system, modification of a single ring substituent led to opposite phase behavior [320].

Adding to the complexity of the phase relationship, it was observed that at high irradiation power ($>300 \text{ W/cm}^2$) the behavior was inverted in amorphous systems [312]. Single-beam experiments at high power showed a central peak instead of a depression. By exposing a sample to a gradient two-beam intersection, a film was inscribed with a continuum of laser intensities. An in-phase grating was found in the high-power region and a conventional out-of-phase SRG in the low-power region. The intermediate region clearly showed interdigitation of the peaks from the two regimes, resembling a doubling of grating period observed by others. These double-period gratings can be formed in a number of amorphous systems, using the polarization combinations of (p, p) or $(+45^\circ, -45^\circ)$, with indications that even the (s, s) and (p, s) combinations function to a certain extent [322–325]. Observations of a double-frequency orientational grating underneath a normal surface relief grating have also been reported [326]. The double-period surface relief gratings were attributed to interference between the diffracted beams from the primary grating, which gives rise to a light modulation, with double the initial frequency, in the material. Whether these double-period gratings are related to the inverted structures observed in high-intensity experiments and some LC systems is an open question. It is interesting to note that some of the amorphous polymers that exhibit double-frequency behavior have accessible LC phases at higher temperature. Combined, these phase behavior results strongly suggest that there are (at least) two mechanisms at play during surface patterning. One dominates at low intensity in amorphous systems, while another appears to dominate at higher intensity and in LC systems. From an applied standpoint, these double-period gratings are of great interest, as they represent a means of generating patterned structures below the usual diffraction limit of far-field optical lithography.

Of considerable importance is the fact that the optical inscription process is sensitive to both intensity and polarization [327]. Different polarization combinations lead to different amplitudes, h , of the inscribed SRG, as shown in Table 1 (the coordinate system is shown in Fig. 15). An optical field vector component in the direction of light modulation (hence mass transport) appears necessary [318]. Interestingly, SRGs can even be formed via pure polarization patterns, where the light intensity is uniform over the sample surface [328].

Table 1. Polarization patterns at the sample surface during SRG inscription using a variety of polarized beam combinations. The ‘quality’ of the SRG (as determined by grating height) is shown for comparison.

Polarization of beams:	Electric Field in xy Plane					SRG Quality
	$x:$	$+\pi$ $+\Lambda/2$	$+\pi/2$ $+\Lambda/4$	0 0	$-\pi/2$ $-\Lambda/4$	
$s : s$ $\updownarrow \updownarrow$	\bullet	\updownarrow	\updownarrow	\updownarrow	\bullet	6 – Poor
$s : p$ $\updownarrow \leftrightarrow$	\swarrow	\circ	\nearrow	\circ	\swarrow	4
$p : p$ $\leftrightarrow \leftrightarrow$ xy plane xz plane	\leftrightarrow \updownarrow	\leftrightarrow \circ	\leftrightarrow \leftrightarrow	\leftrightarrow \circ	\leftrightarrow \updownarrow	3
$+45^\circ : +45^\circ$ $\nearrow \nearrow$	\nearrow	\nearrow	\nearrow	\nearrow	\nearrow	5
$+45^\circ : -45^\circ$ $\nearrow \searrow$	\leftrightarrow	\circ	\updownarrow	\circ	\leftrightarrow	2 – Good
RCP : RCP $\circ \circ$	\circ	\circ	\circ	\circ	\circ	7 – Worst
RCP : LCP $\circ \circ$	\leftrightarrow	\nearrow	\updownarrow	\swarrow	\leftrightarrow	1 – Best

In fact, the (s, s) and (RCP, RCP) combinations, which correspond to mainly variations in intensity and little to no polarization contrast, produce very poor SRGs. By contrast, the best gratings are obtained with $(+45^\circ, -45^\circ)$ and (RCP, LCP) combinations, which involve primarily variation in polarization state across the film. It should be noted, however, that the exact polarization pattern present inside the material is not known. The pattern impinging on the sample is readily calculated from knowledge of the input polarizations, yet in the bulk of the material the light pattern will be redirected and repolarized based on the detailed three-dimensional structure of the surface, refractive index, and birefringence. The optical erasure of an SRG, performed by homogenous irradiation, is also polarization-dependant [329, 330]. Thus, the gratings possess a memory of the polarization state during inscription, encoded in the orientational distribution of chromophores at various grating positions. Typically, gratings inscribed with highly favorable polarization combinations will be optically

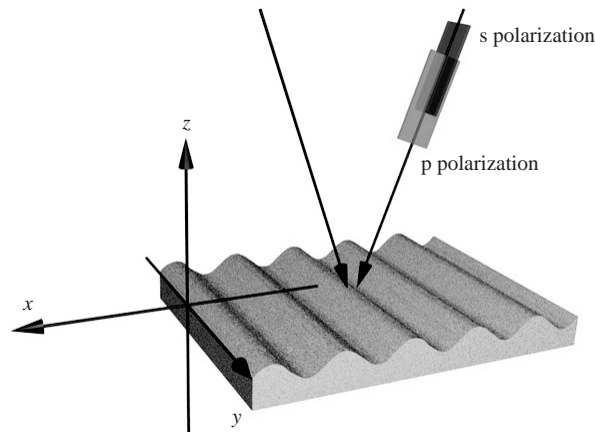


Figure 15. Coordinate system used to describe surface relief grating inscription, with x running along the direction of light modulation. The two incident beams have their polarization state controlled. The s polarization is parallel to the surface, whereas the p state is parallel to the plane-of-incidence.

erased more quickly. The *s*-polarization state, which produces poor gratings, is generally optimal for performing the erasure. These results are obviously related to the orientational distribution of chromophores after surface patterning and their subsequent interaction with the erasing polarization.

4.1.2. Patterning

In a typical inscription experiment, a sinusoidally varying light pattern is generated at the sample surface. What results is a sinusoidal surface profile: a surface relief grating (SRG). This is the pattern most often reported in the literature, because it is conveniently generated (by intersecting two coherent beams) and easily monitored (by recording the diffraction intensity at a nonabsorbing wavelength, usually using a HeNe laser at 633 nm). However, it must be emphasized that the azo surface mass transport can produce arbitrary patterns. Essentially, the film encodes the impinging light pattern as a topography pattern. Both the intensity and the polarization of light are encoded. What appears to be essential is a *gradient* in the intensity and/or polarization of the incident light field. For instance, a single focused Gaussian laser spot will lead to a localized depression, a Gaussian line will lead to an elongated trench, etc. [318]. In principle, any arbitrary pattern could be generated through an appropriate mask, interference/holographic setup, or scanning of a laser spot [185].

Concomitant with the inscription of a surface relief is a photoorientation of the azo chromophores, which depends on the polarization of the incident beam(s). The orientation of chromophores in SRG experiments has been measured using polarized Raman confocal microspectrometry [323, 325, 331]. The strong surface orientation is confirmed by photoelectron spectroscopy [332]. What is found is that the chromophores orient perpendicular to the local polarization vector of the impinging interference pattern. Thus, for a (+45°, -45°) two-beam interference, in the valleys ($x = 0$) the electric field is aligned in the *y*-direction, so the chromophores orient in the *x*-direction, in the peaks ($x = \Lambda/2$) the chromophores orient in the *y*-direction, and in the slope regions ($x = \Lambda/4$) the electric field is circularly polarized and thus the chromophores are nearly isotropic. For a (*p*, *p*) two-beam interference, it is observed that the chromophores are primarily oriented in the *y*-direction everywhere, since the impinging light pattern is always linearly polarized in the *x*-direction. Mass transport may lead to perturbations in the orientational distribution, but photoorientation remains the dominant effect.

The anisotropy grating that is submerged below a surface relief grating apparently leads to the formation of a density grating under appropriate conditions. It was found that upon annealing an SRG, which erases the surface grating and restores a flat film surface, a density grating began growing beneath the surface (and into the film bulk) [333, 334]. This density grating only develops where the SRG was originally inscribed. It appears that the photoorientation and mass transport leads to the nucleation of liquid-crystalline “seeding aggregates” that are thermally grown into larger-scale density variations. The thermal erasure of the SRG, with concomitant growth of the density grating, has been measured [335] and modeled [336]. Separating the components due to the surface relief and the density grating is described in a later section. Briefly, the diffraction of a visible-light laser primarily probes the surface relief, whereas a simultaneous X-ray diffraction experiment probes the density grating. The formation of a density grating is similar to, and consistent with, the production of surface topography [337] and surface density patterns [338], as observed by tapping mode AFM, on an azo film exposed to an optical near-field. In these experiments, it was found that volume is not strictly conserved during surface deformation [339], consistent with changes in density.

4.1.3. Dependence on Material Properties

For all-optical surface patterning to occur, one necessarily requires azobenzene chromophores in some form. There are, however, a wide variety of azo materials that have exhibited surface mass patterning. This makes the process much more attractive from an applied standpoint; it is not merely a curiosity restricted to a single system but rather a fundamental phenomenon that can be engineered into a wide variety of materials. It was

recognized early on that the gratings do not form in systems of small molecules (for instance, comparing unreacted monomers to their corresponding polymers). The polymer molecular weight (MW), however, must not be too large [311]. Presumably a large MW eventually introduces entanglements which act as cross-links, hindering polymer motion. Thus intermediate molecular weight polymers ($MW \sim 10^3$, arguably oligomers) are optimal. That having been said, there are many noteworthy counter examples. Weak SRGs can be formed in polyelectrolyte multilayers, which are essentially cross-linked polymer systems [149, 164, 176, 181]. Efficient grating formation has also been demonstrated using an azo-cellulose with ultra-high molecular weight ($MW \sim 10^7$) [340, 341]. In a high molecular weight polypeptide ($MW \sim 10^5$), gratings could be formed where the grating amplitude was dependant on the polymer conformation [342]. Restricted conformations (α -helices and β -sheets) hindered SRG formation.

The opposite extreme has also been investigated: an amorphous molecular (nonpolymeric) azo with bulky pendants exhibited significant SRG formation [343]. In fact, the molecular version formed gratings more quickly than its corresponding polymer [344]. Another set of experiments compared the formation of gratings in two related arrangements: (1) a thin film of polymer and small-molecule azo mixed together and (2) a layered system, where a layer of the small-molecule azo was deposited on top of the pure polymer [345]. The SRG was negligible in the layered case. Whereas the authors suggest that “layering” inhibits SRG formation, it may be interpreted that coupling to a host polymer matrix enhances mass transport, perhaps by providing rigidity necessary for fixation of the pattern. A copolymer study did in fact indicate that strong coupling of the mesogen to the polymer enhanced SRG formation [346].

Gratings have also been formed in liquid-crystalline systems [319, 320]. In some systems, it was found that adding stoichiometric quantities of a non-azo LC guest greatly improved the grating inscription [347, 348]. This suggests that SRG formation may be an inherently cooperative process, related to the mesogenic nature of the azo chromophore. The inscription sometimes requires higher power ($>1 \text{ W/cm}^2$) than in amorphous systems [349]. In dendrimer systems, the quality of the SRG depends on the generation number [350].

Maximizing the content of azo chromophore usually enhances SRG formation [313], although a copolymer study produced a counter example where intermediate functionalization (50–75%) created the largest SRG [351]. Some attempts have been made to probe the effect of free volume. By attaching substituents to the azo-ring, its steric bulk is increased, which presumably increases the free volume requirement for isomerization. However, substitution also invariably affects the isomerization rate constants, quantum yield, refractive index, etc. This makes any analysis ambiguous. At least in the case of photoorientation, the rate of inscription appears slower for bulkier chromophores, although the net orientation is similar [352, 353]. For grating formation, it would appear that chromophore bulk is of secondary importance to many other inscription parameters. The mass transport occurs readily at room temperature, which is well below the glass-to-rubber transition temperature (T_g) of the amorphous polymers typically used. Gratings can even be formed in polymers with exceptionally high T_g [208], sometimes higher than 370°C [354]. These gratings can sometimes be difficult to erase via annealing [355].

4.1.4. Photosoftening

The formation of an SRG involves massive material motion. It would appear that the process is in some way a surface phenomenon, since non-azo capping layers tend to inhibit the phenomenon [356]. Many other experiments, however, confirm that azos deeper in the film (which still absorb light) contribute to the mass transport [357]. It is clear that the azobenzene isomerization is necessary to permit bulk material flow well below the polymer T_g . It is usually postulated that repeated $\text{trans} \rightarrow \text{cis} \rightarrow \text{trans}$ cycles “photosoften” or “photoplasticize” the polymer matrix, enhancing polymer mobility by orders of magnitude. While this explanation is very compelling, its direct observation has proved ambiguous. Clearly motion is enabled during isomerization, as demonstrated by mass transport, increases in gas permeability [358], the segregation of some material components to the free surface [359], and the ability to optically erase SRGs [314, 329, 330]. The fact that incoherent illumination

during SRG inscription enhances grating formation may also be interpreted as evidence that photosoftering is a dominant requirement for mass transport [360]. Numerous reports have confirmed a reduction in the viscosity of polymer solutions upon *trans* to *cis* conversion [361–363]. This photothinning can be attributed to both chain conformation (reduced hydrodynamic size) and interchain interactions. The extent to which such results can be extended into bulk films is debatable. It is also worth noting that a depression of T_g near the surface of a polymer film is now well-established [364]. One might be tempted to explain the mass transport by suggesting that an ultra-thin layer of polymer material at the surface is sufficiently mobile (below T_g) to move, thereby exposing “fresh surface,” which then becomes mobile. However, the T_g depressions typically measured are not sufficient to account for the process (especially in high- T_g samples). Moreover, this does not explain why the mass patterning is only observed in samples that contain azobenzene.

Despite compelling indirect experiments, there are few results that directly suggest photosoftering in bulk samples. Hints from AFM response [317], experiments with a quartz crystal microbalance [365], and electromechanical spectroscopy [366] all indicate that photosoftering is occurring. However, the magnitude of the effect is quite small and certainly much smaller than the change in mechanical response that occurs upon heating a polymer to T_g . Thus, although mobility appears to be comparable to that of a polymer above T_g , other mechanical properties are only slightly modified. It may indeed be that isomerization merely enables localized molecular motion but that the continual creation of molecular free volume pockets, which are then reoccupied by neighboring isomerizing chromophores, enables a net cooperative movement of material, akin to the displacement of a vacancy defect in a crystal or a hole in a semiconductor [366]. More investigations, for instance using AFM in the force–distance mode [367], may help to settle these questions.

4.1.5. Measuring Gratings

The formation of an SRG is typically monitored via the diffraction of a probe laser beam. One must be careful in analyzing this diffraction efficiency, however, because a number of simultaneous gratings will be generated in an azo sample during illumination with a light pattern (Fig. 16). A light intensity pattern will lead to a chemical grating, since illuminated regions will be more *cis*-rich than dark regions. The resultant spatial variation of absorbance and refractive index will lead to various optical effects, including diffraction. This grating is temporary, persisting only during irradiation. Simultaneously, a birefringence grating will

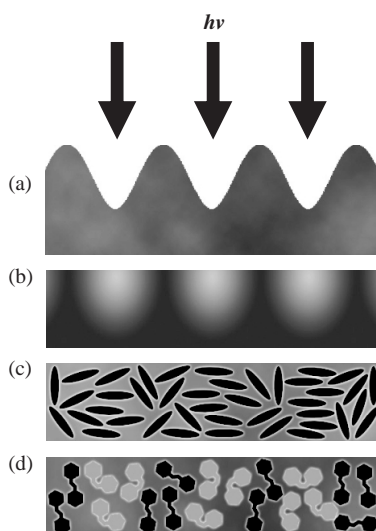


Figure 16. Schematic of the different gratings that are formed during illumination of an azo sample. (a) Surface relief grating (SRG). (b) Density grating (DG). (c) Birefringence (orientational) grating. (d) Chemical (*trans/cis*) grating. All the gratings contribute to the observed diffraction efficiency, to varying extents. Gratings (b), (c) and (d) are all refractive-index gratings.

be inscribed. These birefringence patterns are stable and contribute to the observed final diffraction efficiency. A surface relief grating is of course induced if there is any spatial variation in intensity and/or polarization, and diffraction from this grating is very large, sometimes overwhelming other effects. Lastly, a density grating appears to be seeded beneath the material surface, which will also lead to periodic variation of refractive index.

The contributions to diffraction due to the surface relief and birefringence gratings can be deconvoluted using a Jones matrix formalism applied to polarized measurements of the 1st-order diffracted beams [61, 346, 368–370]. Similarly, scattering theory [336, 371] was used to fit visible-light and X-ray diffraction data [335, 357, 372–374], in order to deconvolute contributions due to surface relief and density (refractive index) gratings. For scattering from an SRG, the x and z components of the momentum transfer are

$$\begin{aligned} q_x &= k(\sin \theta_f - \sin \theta_i) \\ q_z &= nk(\cos \theta_i + \cos \theta_f) \end{aligned} \quad (2)$$

where θ_i and θ_f are the incident and reflected angles and $k = 2\pi/\lambda$. For the visible diffracted peak of order m (i.e., when $q_x = m2\pi/\Lambda$), the scattering intensity was derived to be

$$I_{\text{vis}} \approx |J_m(q_z h) - e^{iq_z d} J_m(q_z \Delta n_m d)|^2 \quad (3)$$

where d is the film thickness, h is the grating height, Δn_m is the m -th Fourier component of the refractive-index grating, and J_m is the m -th Bessel function. These Bessel functions can give rise to oscillations in the diffraction signal (Fig. 17). Thus, one must be careful not to implicitly assume a linear dependence between grating amplitude and diffraction efficiency. Clearly, both the density and surface relief gratings contribute to the signal. For the X-ray signal, the scattering amplitude is given by

$$A_{\text{x-ray}} \approx J_m(q_z h) - e^{iq_z d} \frac{B_m}{2} \quad (4)$$

where one must now use the q_z appropriate for X-rays and B_m represents the Fourier component of the density modulation (which is presumably identical to the index modulation). The intensity is not simply the square of A but can be determined using Fresnel transmission functions. The visible scattering is mostly sensitive to the surface relief, and the X-ray scattering is due primarily to the density modulation. Using both measurements, the two contributions can of course be determined.

It is worth noting that chromophores may actually be disturbed by probe beams that are well outside of the azo absorption window. For instance, it was found that illumination using red light (outside of the azo absorption band) made density gratings (formed underneath surface relief gratings) stable against thermal erasure [334]. Others have found that chromophores become slowly aligned even with red laser light, where absorption should be nominal. Luckily the diffraction from azo gratings is intense, enabling the use of heavily attenuated probe beams.

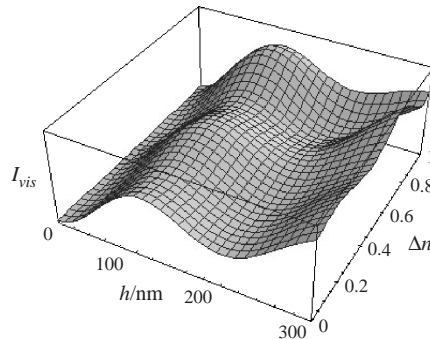


Figure 17. Diffraction intensity of a 700 nm thick film as a function of the inscribed grating height, h , and induced refractive-index grating (Δn), based on equation (3). The diffraction intensity is not a linear function of either variable. Oscillations in the signal can complicate analysis of experiments.

4.1.6. Dynamics

Many dynamic measurements of SRG inscription have been made. To a first approximation, the inscription process does not depend on the temporal distribution of laser power, only on the net exposure. Yet this general rule breaks down at high and low power and for short or interrupted exposures, revealing more complications inherent to the process. The inscription appears to be nonlinear, saturating with inscription time and power and being dependent upon history [375]. Interestingly, the growth of the gratings appears to continue for a short time after illumination has ceased, hinting at a photoinduced stress that persists in the dark. This may be due to the relatively slow decay of the cis population. For short (<2 s) moderate-power laser pulses, no permanent grating can be formed, even after repeated pulse exposure [376]. For longer (>5 s) pulses, material deformation can be seen after every exposure, and repeated exposure eventually leads to an SRG. These short pulses give rise to localized hills that eventually become a smooth sine wave. This implies that with sufficient power, individual azo chromophores or nanodomains deform, which when summed lead to a grating. Although short exposures do not form permanent gratings, some response is seen, possibly indicating elastic deformation [357, 373] in addition to plastic flow.

The formation and erasure of surface relief and density gratings in azo films has been measured and modeled. Using the formalism described in the previous section, one can fit the measured scattering by allowing h and Δn (or B_m) to vary in time. For instance, the erasure of the SRG, and concomitant enhancement and then disappearance of the X-ray signal, can be fit by using [335].

$$h = h_{\max} \frac{1}{1 + \exp\left(\frac{T - C_{\text{SRG}} T_g}{E_{a, \text{SRG}}}\right)}$$

$$B_m = B_{m, \max} \frac{1}{1 + \exp\left(\frac{T - C_{\text{DG}} T_g}{E_{a, \text{DG}}}\right)}$$
(5)

where $E_{a, i}$ and C_i are the activation energy and a fitting parameter, respectively, for the surface relief (SRG) and density (DG) gratings. It is found that the surface relief grating begins disappearing ~ 15 K before T_g . In contrast to this thermal erasure of SRGs, it appears that in some liquid-crystalline systems, thermal treatment after SRG formation leads to an enhancement of the grating height [377, 378]. In these cases, heating may enable motion and aggregation of chromophores.

4.2. Mechanism

Several mechanisms have been described to account for the microscopic origin of the driving force in azobenzene optical patterning. Arguments have appealed to thermal gradients, diffusion considerations, isomerization-induced pressure gradients, and interactions between azo dipoles and the electric field of the incident light. Considering the large body of experimental observations, it is perhaps surprising that the issue of mechanism has not yet been settled. At present, no mechanism appears to provide an entirely complete and satisfactory explanation consistent with all known observations. On the other hand, viscoelastic modeling of the process has been quite successful, correctly reproducing nearly all experimentally observed surface patterns, without directly describing the microscopic nature of the driving force. Fluid mechanics models provided suitable agreement with observations [379] and were later extended to take into account a depth dependence and a velocity distribution in the film [380, 381], which reproduces the thickness dependence of SRG inscription. A further elaboration took into account induced anisotropy in the film and associated anisotropic polymer film deformation (expansion or contraction in the electric field direction) [382]. The assumption of an anisotropic deformation is very much consistent with experimental observations [277]. Such an analysis, remarkably, reproduced most of the polarization dependence, predicted phase-inverted behavior at high power, and even demonstrated double-period (interdigitated) gratings. A nonlinear stress-relaxation analysis could account for the nonlinear response during intermittent (pulse-like) exposure [375]. Finite-element linear

viscoelastic modeling enabled the inclusion of finite compressibility [383]. This allowed the nonlinear intermittent-exposure results and, critically, the formation of density gratings, to be correctly predicted. This analysis also demonstrated, as expected, that surface tension acts as a restoring force that limits grating amplitude (which explains the eventual saturation). Finally, the kinetics of grating formation (and erasure) have been captured in a lattice Monte Carlo simulation that takes into account isomerization kinetics and angular redistribution of chromophores [384–386]. Thus, the nonlinear viscoelastic flow and deformation (compression and expansion) of polymer material appear to be well-understood. What remains to be fully elucidated is the origin of the force inside the material. More specifically, the connection between the azobenzene isomerization and the apparent force must be explained.

4.2.1. Thermal Considerations

Models involving thermal effects were proposed when SRG formation was first observed. Although simple and appealing, a purely thermal mechanism would not account for the polarization dependence that is observed experimentally. The grating formation proceeds at remarkably low laser power, thus thermal mechanisms appear untenable. A more detailed modeling analysis [387] showed that the temperature gradient induced in a sample under typical SRG formation conditions was on the order of 10^{-4} K. This thermal gradient is much too small for any appreciable spatial variation of material properties. The net temperature rise in the sample was found to be on the order of 5 K, which again suggests that thermal effects (such as temperature-induced material softening) are negligible. On the other hand, high-intensity experiments have shown the formation of gratings that could not be subsequently thermally erased [312]. It is likely that in these cases a destructive thermal mechanism plays a role. In nanosecond pulsed experiments, gratings can be formed [388–391]. However, these gratings are due to irreversible ablation of the sample surface, a phenomenon well established in high-power laser physics. Moreover, the formation of gratings at these energies does not require azobenzene: any absorbing chromophore will do [392]. Computer modeling confirms temperature rises on the order of ~ 8000 K for nanosecond pulses [387], clearly an entirely different regime from the facile room-temperature patterning unique to azo chromophores. Although thermal effects should be considered for a complete understanding of SRG formation (especially the phase-inverted structures observed at higher power), they appear to be negligible for typical irradiation conditions at modest laser power.

4.2.2. Asymmetric Diffusion

An elegant anisotropic translation mechanism was developed by Lefin, Fiorini, and Nunzi [393, 394]. In this model, material transport occurs essentially due to an (orientational) concentration gradient. It is suggested that the rapid cycling of chromophores between trans and cis states enables transient, random motion of molecules preferentially along their long axis, due to the inherent anisotropy of azo molecules. The probability of undergoing a random-walk step is proportional to the probability of isomerization, which of course depends upon the light intensity and the angle between the chromophore dipole and the incident electric vector. This predicts a net flux of molecules out of the illuminated areas and into the dark regions, consistent with experiment. This process would be enhanced by pointing dipoles in the direction of the light gradient (towards the dark regions). This would appear to explain the polarization dependence to a certain extent. In contrast to experiment, however, this model implies the best results when using small molecules, not polymers. For polymer chains laden with many chromophores, random motion of these moieties would presumably lead to a “tug-of-war” that would defeat net transport of the chain. It is at present not clear that the driving force in this model is sufficient to account for the substantial mass transport (well below T_g) observed in experiments.

4.2.3. Mean-Field Theory

Mechanisms based on electromagnetic forces are promising, since they naturally include the intensity and polarization state of the incident light field. In the mean-field model developed by Pedersen et al. [395, 396], each chromophore is subject to a potential resulting from all

the other chromophore dipoles in the material. Irradiation orients chromophores, and this net orientation leads to a potential that naturally aligns other chromophores. Furthermore, there is an attractive force between side-by-side chromophores that are aligned similarly. This leads to a net force on chromophores in illuminated areas, causing them to order and aggregate. Obviously this model predicts an accumulation of chromophores in the illuminated areas. Thus surface relief peaks will be aligned with light intensity maxima. While this result does not agree with experiments in amorphous samples, it is consistent with many experiments on LC systems. The mean-field model inherently includes intermolecular cooperativity and orientational order, and it appears natural that it would be manifest in mobile liquid-crystalline systems. The polarization state of incident light is explicitly included in the model, as it serves to align dipoles and thus enhance the mean-field force. Because of this, even pure polarization patterns lead to gratings in this model. This mechanism appeals to the unique properties of azobenzenes only to explain the photoorientation of dipoles. If this mechanism is general, one would expect it to operate on nonisomerizing dipoles that had been aligned by other means, which has not yet been observed.

4.2.4. Permittivity Gradient Theory

A mechanism involving spatial variation of the permittivity, ϵ , has been suggested by Baldus and Zilker [397]. This model assumes that a spatial modulation of the refractive index, hence permittivity, is induced in the film. This is certainly reasonable given the well-known photoorientation and birefringence gratings in azo systems. A force is then exerted between the optical electric field and the gradient in permittivity. Specifically, the force is proportional to the intensity of the electric field in the mass transport direction and to the gradient of the permittivity:

$$\bar{f} = -\frac{\epsilon_0}{2} \bar{E}^2 \nabla \epsilon \quad (6)$$

Mass is thus driven out of areas with a strong gradient in ϵ , which in general moves material into the dark (consistent with the phase relationship in amorphous systems). Here again the mechanism appears general: any system with spatial variation of refractive index should be photopatternable, yet this is not observed. This model would appear to require that adequate photoorientation precede mass transport. Most experiments indicate, however, that both orientational and surface relief phenomena begin immediately and continue concurrently throughout inscription. This model was used to explain SRG formation in pulsed experiments [390, 392], where thermal effects were suggested as giving rise to the spatial variation of permittivity, but the resulting force was essentially identical. However, conventional laser ablation appears to be a simpler explanation for those results [387].

4.2.5. Gradient Electric Force

A mechanism was proposed by Kumar et al. based on the observation that an electric field component in the direction of mass flow was required [317, 328, 398]. This force is essentially an optical gradient force [399–401]. Spatial variation of the light (electric field intensity and orientation) leads to a variation of the material susceptibility, χ , at the sample surface. The electric field then polarizes the material. The induced polarization is related to the light intensity and local susceptibility:

$$\bar{P}_i = \epsilon_0 \chi_{ij} \bar{E}_j \quad (7)$$

Forces then occur between the polarized material and the light field, analogous to the net force on an electric dipole in an electric field gradient. The time averaged force was derived to be [328]

$$\bar{f} = \langle (\bar{P} \cdot \nabla) \bar{E} \rangle \quad (8)$$

The grating inscription is related to the spatially varying material susceptibility, the magnitude of the electric field, and the gradient of the electric field. This theory was extended to include near-field optical gradient forces, which have been used for patterning in some

experiments [402]. The gradient force model naturally includes the polarization dependence of the incident light and reproduces essentially all of the polarization features of single-beam and SRG experiments. It has been pointed out [185], however, that another analysis [403] of forces exerted on polarizable media suggested a dependence on the gradient of the electric field, but not its polarization direction. The gradient force theory requires azobenzene photochemistry to modulate susceptibility via photo-orientation and also implicitly assumes that “photoplasticization” is enabling mass transport. It would appear, however, that the force density predicted by this model is much too small to account for mass transport in real systems. A straightforward analysis presented by Saphiannikova et al. [383] is described here. In the case of two circularly polarized beams (for instance), the force acting in the x -direction, according to the gradient electric force model, would be

$$f = -k\varepsilon_0\chi E_0^2 \sin\theta(1 + \cos^2\theta) \sin(kx \sin\theta) \quad (9)$$

where 2θ is the angle between the two beams and $k = 2\pi/\lambda$. Since $E_0^2 = 2Iz_0$, where z_0 is the vacuum impedance and I is the light intensity, the maximum expected force is

$$f_{\max} = \frac{4\pi}{\lambda} \varepsilon_0 z_0 \chi I \quad (10)$$

Given that $\varepsilon_0 = 8.854 \times 10^{-12} \text{ C}^2/(\text{Nm}^2)$, $|\chi| \approx 1$, and $z_0 = 377 \text{ } \Omega$ and using the typical values $I = 100 \text{ mW/cm}^2$ and $\lambda = 488 \text{ nm}$, we obtain a force density of $\sim 100 \text{ N/m}^3$. Not only is this 2 orders of magnitude smaller than the force of gravity (which itself is presumably negligible), but it falls short of the estimated 10^{11} – 10^{14} N/m^3 necessary for mass transport in polymer films to occur [383].

4.2.6. Isomerization Pressure

One of the first mechanisms to be presented was the suggestion by Barrett et al. of pressure gradients inside the polymer film [311, 379]. The assumption is that azobenzene isomerization generates pressure due both to the greater free volume requirement of the *cis* and to the volume requirement of the isomerization process itself. Isomerization of the bulky chromophores leads to pressure that is proportional to light intensity. The light intensity gradient thus generates a pressure gradient, which of course leads to material flow in a fluid mechanics treatment. Order-of-magnitude estimates were used to suggest that the mechanical force of isomerization would be greater than the yield point of the polymer, enabling flow. Plastic flow is predicted to drive material out of the light, consistent with observations in amorphous systems. At first it would seem that this mechanism cannot be reconciled with the polarization dependence, since the pressure is presumably proportional to light intensity, irrespective of its polarization state. However, one must more fully take orientational effects into account. Linearly polarized light addresses fewer chromophores than circularly polarized light and would thus lead to lower pressure. Thus, pure polarization patterns can still lead to pressure gradients. Combined with the fact that the polarized light is orienting (and in a certain sense photobleaching), this can explain some aspects of the polarization data. The agreement, however, is not perfect. For instance, the (*s*, *s*) and (*p*, *p*) combinations lead to very different gratings in experiments. It is possible that some missing detail related to polarization will help explain this discrepancy.

Combining a variety of results from the literature, it now appears the mechanical argument of a pressure mechanism may be correct. In one experiment, irradiation of a transferred Langmuir–Blodgett film reversibly generated $\sim 5 \text{ nm}$ “hills,” attributed to nanoscale buckling that relieves the stress induced by lateral expansion [404]. This result is conspicuously similar to the spontaneous polarization-dependant formation of hexagonally arranged $\sim 500 \text{ nm}$ hills seen on an amorphous azo-polymer sample irradiated homogeneously [405, 406]. In fact, homogeneous illumination of azo surfaces has caused roughening [366] and homogeneous optical erasure of SRGs leads to similar pattern formation [330]. The early stages of SRG formation, imaged by AFM, again show the formation of nanometer-sized hills [376]. Taken together, these seem to suggest that irradiation of an azo film leads to spontaneous lateral expansion, which induces a stress that can be relieved by buckling of the

surface, thereby generating surface structures. In the case of a light gradient, the buckling is relieved by mass transport coincident with the light field that generated the pressure inside the film. In an experiment on main-chain versus side-chain azo-polymers, the polarization behavior of photodeformation was opposite [339]. This may be explained by postulating that the main-chain polymer contracts upon isomerization, whereas the side-chain polymer architecture leads to net expansion. Similarly, the opposite phase behavior in amorphous and LC systems may be due to the fact that the former photoexpand and the latter photocontract [277]. Lastly, many large surface structures were observed in an azo-dye-doped elastomer film irradiated at high power (4 W/cm^2) [407]. The formation of structures both parallel and perpendicular to the grating direction could be attributed to photoaggregation of the azo dye molecules and/or buckling of the elastomeric surface. Thus a purely photomechanical explanation may be able to describe surface mass transport in azo systems. Further investigations into reconciling this model with the polarization dependence of inscription are in order. Presumably photo-orientation will play a key role.

4.3. Applications of Surface Mass Transport

The rapid, facile, reversible, and single-step all-optical surface patterning effect discovered in a wide variety of azobenzene systems has, of course, been suggested as the basis for numerous applications. Azobenzene is versatile, amenable to incorporation in a wide variety of materials. The mass patterning is reversible, which is often advantageous. On the other hand, one may use a system where cross-linking enables permanent fixation of the surface patterns [408]. Many proposed applications are optical and fit well with azobenzene's already extensive list of optical capabilities. The gratings have been demonstrated as optical polarizers [409], angular or wavelength filters [410, 411], and couplers for optical devices [412]. They have also been suggested as photonic band gap materials [413] and have been used to create lasers where emission wavelength is tunable via grating pitch [414, 415]. The process has, of course, been suggested as an optical data storage mechanism [416]. The high-speed and single-step holographic recording has been suggested to enable "instant holography" [389], with obvious applications for industry or end consumers. Since the hologram is topographical, it can easily be used as a master to create replicas via molding. The surface patterning also allows multiple holograms to be superimposed, if desired. A novel suggestion is to use the patterning for rapid prototyping of optical elements [417]. Optical elements could be generated or modified quickly and during device operation. They could thereafter be replaced with permanent components, if required.

The physical structure of the surface relief can be exploited to organize other systems. For instance, it can act as a command layer, aligning liquid crystals [418–422]. The grating can be formed after the LC cell has been assembled and can be erased and rewritten. Colloids can also be arranged into the grooves of an SRG, thereby templating higher order structures [423, 424]. These lines of colloids can then be sintered to form wires [425]. The surface topography inscription process is clearly amenable to a variety of optical-lithography patterning schemes. These possibilities will hopefully be more thoroughly investigated. One advantage of holographic patterning is that there is guaranteed registry between features over macroscopic distances. This is especially attractive as technologies move towards wiring nanometer-sized components. One example in this direction involved evaporating metal onto an SRG and then annealing. This formed a large number of very long (several millimeters) but extremely thin (200 nm) parallel metal wires [426]. Of interest for next-generation patterning techniques is the fact that the azo surface modification is amenable to near-field patterning, which enables high-resolution nanopatterning by circumventing the usual diffraction limit of far-field optical systems. Proof of principle was demonstrated by irradiating through polystyrene spheres assembled on the surface of an azo film. This results in a polarization-dependent surface topography pattern [337] and a corresponding surface density pattern [338]. Using this technique, resolution on the order of 20 nm was achieved [427]. This process appears to be enhanced by the presence of gold nanoislands [428]. It was also shown that volume is not strictly conserved in these surface deformations [339]. In addition to being useful as a sub-diffraction limit patterning technique, it should be noted that this

is also a useful technique for imaging the near-field of various optical interactions [429]. The (as of yet not fully explained) fact that sub-diffraction limit double-frequency surface relief gratings can be inscribed via far-field illumination [322–325] further suggests the azo-polymers as versatile high-resolution patterning materials.

5. CONCLUSIONS

Azobenzene polymers are versatile and functional materials that exhibit photoresponsive behavior not seen in any other system. They are fundamentally interesting as optical materials. As already described, azo materials have been demonstrated as waveguides, polarization filters, couplers, nonlinear devices, data storage elements, etc. More significant than the mere demonstration of all these optical components is the ability to induce them all in a single material. Thus, azo-polymers have often been viewed as a future all-in-one scaffold for optical processing, i.e., the optical analogue of an integrated chip. This is a promising possibility for the future that has not been sufficiently investigated. So far, there has been no convincing demonstration that all these effects can be conveniently combined in a single film, using a procedure that is inherently scalable. It remains to be seen if azo-polymers will emerge as the scaffold of choice for next-generation optical systems.

In addition to being useful in a variety of photoswitching roles, the azobenzene isomerization, being fundamentally a geometrical motion, can give rise to many types of motion. These motions can lead to formation of structures at a variety of length scales, from molecular to macroscopic. Furthermore, the formation of these structures is optically controlled, which is very attractive to modern industry. At a molecular level, there is much promise in exploiting azobenzenes to control the organization of nanomaterials and the functioning of nano-mechanical devices. At a nanometer level, these materials can be used to form arbitrary surface patterns in a single-step process. At a macroscopic level, the motion could be exploited in a variety of photoactuators and artificial muscles.

With regard to the mechanism of surface mass transport, there is a need for further theory and experiments. An emerging possibility is that two competing mechanisms apply at different power levels. In some systems, notably liquid-crystalline ones, motion is sufficiently free that the “high-power” mechanism is readily accessible. Such an interpretation seems to resolve the apparent conflict between many different results. The nature of the two mechanisms, of course, remains an open question. The high-power mechanism may be due to mean-field forces. Again, in mobile LC systems, or at sufficient power, one might expect molecules to align, attract one another, and move cooperatively. In the low-power regime, a photomechanical mechanism appears tenable, although polarization questions need to be addressed, presumably by appealing to photo-orientation phenomena. From an applied perspective, the azo-polymers are ideal for high-performance optical lithography. Specifically, these materials have been patterned at the sub-diffraction limit level, thus showing that any material resolution limits are below the usual optical limits. The double period gratings that have been produced show that these systems are amenable to sub-diffraction limit patterning even with far-field illumination. Ongoing research is evaluating these effects in terms of facile optical formation of nanostructures.

REFERENCES

1. H. Zollinger, “Azo and Diazo Chemistry.” Interscience, New York, 1961.
2. H. Zollinger, “Colour Chemistry, Synthesis, Properties, and Applications of Organic Dyes.” VCH, Weinheim, 1987.
3. S. Kwolek, P. Morgan, and J. Schaeffgen, “Encyclopedia of Polymer Science and Engineering.” Vol. 9, John Wiley, New York, 1985.
4. G. Möhlmann and C. van der Vorst, “Side Chain Liquid Crystal Polymers” (C. Mardle, Plenum, and Hall, Ed.), Glasgow, 1989.
5. H. Rau, in “Photochemistry and Photophysics” (J. Rebek, Ed.), Vol. 2, pp. 119–141, CRC Press, Boca Raton, FL, 1990.
6. H. Rau, *Ber. Bunsen-Ges.* 72, 408 (1968).
7. J. A. Delaire and K. Nakatani, *Chem. Rev.* 100, 1817 (2000).
8. F. W. Schulze, H. J. Petrick, H. K. Cammenga, and H. Klinge, *Z. Phys. Chem.* 107, 1 (1977).

9. I. Mita, K. Horie, and K. Hirao, *Macromolecules* 22, 558 (1989).
10. S. Monti, G. Orlandi, and P. Palmieri, *Chem. Phys.* 71, 87 (1982).
11. T. Kobayashi, E. O. Degenkolb, and P. M. Rentzepis, *J. Phys. Chem.* 83, 2431 (1979).
12. I. K. Lednev, T.-Q. Ye, R. E. Hester, and J. N. Moore, *J. Phys. Chem.* 100, 13338 (1996).
13. L. Lamarre and C. S. P. Sung, *Macromolecules* 16, 1729 (1983).
14. Y. Shirota, K. Moriwaki, S. Yoshikawa, T. Ujike, and H. Nakano, *J. Mater. Chem.* 8, 2579 (1998).
15. B. K. Kerzhner, V. I. Kofanov, and T. L. Vrubel, *Zh. Obshch. Khim.* 53, 2303 (1983).
16. U. Funke and H. F. Gruetzmacher, *Tetrahedron* 43, 3787 (1987).
17. G. S. Hartley, *Nature* 140, 281 (1937).
18. G. S. Hartley, *J. Chem. Soc. Abstr.* 633 (1938).
19. E. Fischer, *J. Phys. Chem.* 71, 3704 (1967).
20. H. Rau, G. Greiner, G. Gauglitz, and H. Meier, *J. Phys. Chem.* 94, 6523 (1990).
21. G. Gabor and E. Fischer, *J. Phys. Chem.* 75, 581 (1971).
22. C. D. Eisenbach, *Macromol. Rapid Commun.* 1, 287 (1980).
23. S. R. Hair, G. A. Taylor, and L. W. Schultz, *J. Chem. Educ.* 67, 709 (1990).
24. P. L. Beltrame, E. D. Paglia, A. Castelli, G. F. Tantardini, A. Seves, and B. Marcandalli, *J. Appl. Polym. Sci.* 49, 2235 (1993).
25. S. Xie, A. Natansohn, and P. Rochon, *Chem. Mater.* 5, 403 (1993).
26. D. Gegiou, K. A. Muszkat, and E. Fischer, *J. Am. Chem. Soc.* 90, 3907 (1968).
27. H. Rau and E. Lueddecke, *J. Am. Chem. Soc.* 104, 1616 (1982).
28. T. Naito, K. Horie, and I. Mita, *Macromolecules* 24, 2907 (1991).
29. Z. F. Liu, K. Morigaki, T. Enomoto, K. Hashimoto, and A. Fujishima, *J. Phys. Chem.* 96, 1875 (1992).
30. A. Altomare, F. Ciardelli, N. Tirelli, and R. Solaro, *Macromolecules* 30, 1298 (1997).
31. T. Fujino and T. Tahara, *J. Phys. Chem. A* 104, 4203 (2000).
32. T. Fujino, S. Y. Arzhantsev, and T. Tahara, *J. Phys. Chem. A* 105, 8123 (2001).
33. C.-H. Ho, K.-N. Yang, and S.-N. Lee, *J. Polym. Sci. Part A: Polym. Chem.* 39, 2296 (2001).
34. C. Angeli, R. Cimraglia, and H.-J. Hofmann, *Chem. Phys. Lett.* 259, 276 (1996).
35. B. S. Jursic, *Chem. Phys. Lett.* 261, 13 (1996).
36. T. Ikeda and O. Tsutsumi, *Science* 268, 1873 (1995).
37. W. J. Priest and M. M. Sifain, *J. Polym. Sci., Polym. Chem. Ed.* 9, 3161 (1971).
38. C. S. Paik and H. Morawetz, *Macromolecules* 5, 171 (1972).
39. C. Barrett, A. Natansohn, and P. Rochon, *Chem. Mater.* 7, 899 (1995).
40. C. Barrett, A. Natansohn, and P. Rochon, *Macromolecules* 27, 4781 (1994).
41. N. Sarkar, A. Sarkar, and S. Sivaram, *J. Appl. Polym. Sci.* 81, 2923 (2001).
42. L. L. Norman and C. J. Barrett, *J. Phys. Chem. B* 106, 8499 (2002).
43. K. Tanaka, Y. Tateishi, and T. Nagamura, *Macromolecules* 37, 8188 (2004).
44. H. Rau, A. D. Crosby, A. Schaufler, and R. Frank, *Z. Naturforsch. A: Phys. Sci.* 36, 1180 (1981).
45. S. Malkin and E. Fischer, *J. Phys. Chem.* 66, 2482 (1962).
46. Y. Q. Shen and H. Rau, *Macromol. Chem. Phys.* 192, 945 (1991).
47. P. Bortolus and S. Monti, *J. Phys. Chem.* 83, 648 (1979).
48. S. Yitzchaik and T. J. Marks, *Acc. Chem. Res.* 29, 197 (1996).
49. D. Levy and L. Esquivias, *Adv. Mater.* 7, 120 (1995).
50. M. Sisido, Y. Ishikawa, M. Harada, and K. Itoh, *Macromolecules* 24, 3999 (1991).
51. I. Willner and S. Rubin, *Angew. Chem. Int. Ed. Engl.* 35, 367 (1996).
52. B. Gallot, M. Fafiotte, A. Fissi, and O. Pieroni, *Macromol. Rapid Commun.* 17, 493 (1996).
53. S. Shinkai, T. Minami, Y. Kusano, and O. Manabe, *J. Am. Chem. Soc.* 105, 1851 (1983).
54. J. H. Jung, C. Takehisa, Y. Sakata, and T. Kaneda, *Chem. Lett.* 147 (1996).
55. H. Yamamura, H. Kawai, T. Yotsuya, T. Higuchi, Y. Butsugan, S. Araki, M. Kawai, and K. Fujita, *Chem. Lett.* 799 (1996).
56. A. K. Singh, J. Das, and N. Majumdar, *J. Am. Chem. Soc.* 118, 6185 (1996).
57. S. H. Chen, J. C. Mastrangelo, H. Shi, T. N. Blanton, and A. Bashir-Hashemi, *Macromolecules* 30, 93 (1997).
58. S. H. Chen, J. C. Mastrangelo, H. Shi, A. Bashir-Hashemi, J. Li, and N. Gelber, *Macromolecules* 28, 7775 (1995).
59. K. Ichimura, *Chem. Rev.* 100, 1847 (2000).
60. R. Birabassov, N. Landraud, T. V. Galstyan, A. Ritcey, C. G. Bazuin, and T. Rahem, *Appl. Opt.* 37, 8264 (1998).
61. F. L. Labarthe, T. Buffeteau, and C. Sourisseau, *J. Phys. Chem. B* 102, 2654 (1998).
62. N. K. Viswanathan, D. Y. Kim, S. Bian, J. Williams, W. Liu, L. Li, L. Samuelson, J. Kumar, and S. K. Tripathy, *J. Mater. Chem.* 9, 1941 (1999).
63. A. Natansohn, P. Rochon, J. Gosselin, and S. Xie, *Macromolecules* 25, 2268 (1992).
64. M. S. Ho, C. Barrett, J. Paterson, M. Esteghamatian, A. Natansohn, and P. Rochon, *Macromolecules* 29, 4613 (1996).
65. X. Wang, J.-I. Chen, S. Marturunkakul, L. Li, J. Kumar, and S. K. Tripathy, *Chem. Mater.* 9, 45 (1997).
66. X. Wang, J. Kumar, S. K. Tripathy, L. Li, J.-I. Chen, and S. Marturunkakul, *Macromolecules* 30, 219 (1997).
67. X. Wang, S. Balasubramanian, L. Li, X. Jiang, D. J. Sandman, M. F. Rubner, J. Kumar, and S. K. Tripathy, *Macromol. Rapid Commun.* 18, 451 (1997).
68. F. Agolini and F. P. Gay, *Macromolecules* 3, 349 (1970).
69. K. Anderle, R. Birenheide, M. Eich, and J. H. Wendorff, *Makromol. Chem. Rapid Commun.* 10, 477 (1989).

70. J. Furukawa, S. Takamori, and S. Yamashita, *Angew. Makromol. Chem.* 1, 92 (1967).
71. M. C. Bignozzi, S. A. Angeloni, M. Laus, L. Incicco, O. Francescangeli, D. Wolff, G. Galli, and E. Chiellini, *Polym. J. (Tokyo)* 31, 913 (1999).
72. X.-H. Liu, D. W. Bruce, and I. Manners, *Chem. Commun.* 289 (1997).
73. H. B. Meikelburger, K. Rissanen, and F. Voegtle, *Chem. Ber.* 126, 1161 (1993).
74. D. M. Junge and D. V. McGrath, *Chem. Commun.* 857 (1997).
75. M. Sukwattanasinitt, X. Wang, L. Li, X. Jiang, J. Kumar, S. K. Tripathy, and D. J. Sandman, *Chem. Mater.* 10, 27 (1998).
76. M. Teraguchi and T. Masuda, *Macromolecules* 33, 240 (2000).
77. A. Izumi, M. Teraguchi, R. Nomura, and T. Masuda, *J. Polym. Sci. Part A: Polym. Chem.* 38, 1057 (2000).
78. A. Izumi, M. Teraguchi, R. Nomura, and T. Masuda, *Macromolecules* 33, 5347 (2000).
79. S. Y. Morino, A. Kaiho, and K. Ichimura, *Appl. Phys. Lett.* 73, 1317 (1998).
80. A. Altomare, F. Ciardelli, B. Gallot, M. Mader, R. Solaro, and N. Tirelli, *J. Polym. Sci. Part A: Polym. Chem.* 39, 2957 (2001).
81. N. Tsutsumi, S. Yoshizaki, W. Sakai, and T. Kiyotsukuri, *MCLC S&T, Sect. B: Nonlinear Optics* 15, 387 (1996).
82. K. Ichimura, M. Momose, K. Kudo, H. Akiyama, and N. Ishizuki, *Thin Solid Films* 284, 557 (1996).
83. K. Weh, M. Noack, R. Ruhmann, K. Hoffmann, P. Toussaint, and J. Caro, *Chem. Eng. Technol.* 21, 408 (1998).
84. L. M. Blinov, M. V. Kozlovsky, M. Ozaki, K. Skarp, and K. Yoshino, *J. Appl. Phys.* 84, 3860 (1998).
85. M. Han and K. Ichimura, *Macromolecules* 34, 82 (2001).
86. T. Seki, M. Sakuragi, Y. Kawanishi, T. Tamaki, R. Fukuda, K. Ichimura, and Y. Suzuki, *Langmuir* 9, 211 (1993).
87. G. Jianhua, L. Hua, L. Lingyun, L. Bingjie, C. Yiwen, and L. Zuhong, *Supramol. Sci.* 5, 675 (1998).
88. J. Razna, P. Hodge, D. West, and S. Kucharski, *J. Mater. Chem.* 9, 1693 (1999).
89. J. R. Silva, F. F. Dall'Agnol, O. N. Oliveira, Jr., and J. A. Giacometti, *Polymer* 43, 3753 (2002).
90. S. D. Evans, S. R. Johnson, H. Ringsdorf, L. M. Williams, and H. Wolf, *Langmuir* 14, 6436 (1998).
91. V. Shibaev, A. Bobrovsky, and N. Boiko, *Prog. Polym. Sci.* 28, 729 (2003).
92. S. T. Sun, W. M. Gibbons, and P. J. Shannon, *Liq. Cryst.* 12, 869 (1992).
93. K. Anderle, R. Birenheide, M. J. A. Werner, and J. H. Wendorff, *Liq. Cryst.* 9, 691 (1991).
94. W. M. Gibbons, P. J. Shannon, S.-T. Sun, and B. J. Swetlin, *Nature* 351, 49 (1991).
95. K. Ichimura, Y. Hayashi, H. Akiyama, T. Ikeda, and N. Ishizuki, *Appl. Phys. Lett.* 63, 449 (1993).
96. A. G. Chen and D. J. Brady, *Appl. Phys. Lett.* 62, 2920 (1993).
97. U. Wiesner, N. Reynolds, C. Boeffel, and H. W. Spiess, *Makromol. Chem., Rapid Commun.* 12, 457 (1991).
98. J. Stumpe, L. Mueller, D. Kreysig, G. Hauck, H. D. Koswig, R. Ruhmann, and J. Ruebner, *Makromol. Chem. Rapid Commun.* 12, 81 (1991).
99. S. Hvilsted, F. Andruzzi, C. Kulinna, H. W. Siesler, and P. S. Ramanujam, *Macromolecules* 28, 2172 (1995).
100. O. Yaroschuk, T. Sergan, J. Lindau, S. N. Lee, J. Kelly, and L.-C. Chien, *J. Chem. Phys.* 114, 5330 (2001).
101. M. Eich and J. Wendorff, *J. Opt. Soc. Am. B* 7, 1428 (1990).
102. T. Ikeda, S. Horiuchi, D. B. Karanjit, S. Kurihara, and S. Tazuke, *Macromolecules* 23, 42 (1990).
103. T. Hayashi, H. Kawakami, Y. Doke, A. Tsuchida, Y. Onogi, and M. Yamamoto, *Eur. Polym. J.* 31, 23 (1995).
104. T. Kato, N. Hirota, A. Fujishima, and J. M. J. Frechet, *J. Polym. Sci. Part A: Polym. Chem.* 34, 57 (1996).
105. P. J. Shannon, W. M. Gibbons, and S. T. Sun, *Nature* 368, 532 (1994).
106. Y.-Y. Luk and N. L. Abbott, *Science* 301, 623 (2003).
107. T. Ikeda, T. Sasaki, and K. Ichimura, *Nature* 361, 428 (1993).
108. B. Fischer, C. Thieme, T. M. Fischer, F. Kremer, T. Oge, and R. Zentel, *Liq. Cryst.* 22, 65 (1997).
109. O. Villavicencio and D. V. McGrath, *Adv. Dendritic Macromol.* 5, 1 (2002).
110. A. Momotake and T. Arai, *Polymer* 45, 5369 (2004).
111. A. Momotake and T. Arai, *J. Photochem. Photobiol. C* 5, 1 (2004).
112. D.-L. Jiang and T. Aida, *Nature* 388, 454 (1997).
113. T. Aida, D.-L. Jiang, E. Yashima, and Y. Okamoto, *Thin Solid Films* 331, 254 (1998).
114. D. M. Junge and D. V. McGrath, *J. Am. Chem. Soc.* 121, 4912 (1999).
115. S. Li and D. V. McGrath, *J. Am. Chem. Soc.* 122, 6795 (2000).
116. G. Decher and J. D. Hong, *Ber. Bunsen-Ges.* 95, 1430 (1991).
117. G. Decher and J. Schmitt, *Prog. Colloid Polym. Sci.* 89, 160 (1992).
118. G. Decher, J. D. Hong, and J. Schmitt, *Thin Solid Films* 210–211, 831 (1991).
119. G. Decher, *Science* 277, 1232 (1997).
120. W. Knoll, *Curr. Opin. Colloid Interface Sci.* 1, 137 (1996).
121. G. Decher, M. Eckle, J. Schmitt, and B. Struth, *Curr. Opin. Colloid Interface Sci.* 3, 32 (1998).
122. P. T. Hammond, *Curr. Opin. Colloid Interface Sci.* 4, 430 (1999).
123. G. B. Sukhorukov, J. Schmitt, and G. Decher, *Ber. Bunsen-Ges.* 100, 948 (1996).
124. M. Lösche, J. Schmitt, G. Decher, W. G. Bouwman, and K. Kjaer, *Macromolecules* 31, 8893 (1998).
125. M. R. Linfood, M. Auch, and H. Möhwald, *J. Am. Chem. Soc.* 120, 178 (1998).
126. R. Steitz, V. Leiner, R. Siebrecht, and R. V. Klitzing, *Colloids Surf. A* 163, 63 (2000).
127. S. S. Shiratori and M. F. Rubner, *Macromolecules* 33, 4213 (2000).
128. A. J. Chung and M. F. Rubner, *Langmuir* 18, 1176 (2002).
129. T. C. Wang, M. F. Rubner, and R. E. Cohen, *Langmuir* 18, 3370 (2002).
130. S. E. Burke and C. J. Barrett, *Langmuir* 19, 3297 (2003).
131. S. T. Dubas and J. B. Schlenoff, *Macromolecules* 32, 8153 (1999).
132. H. H. Rmaile and J. B. Schlenoff, *J. Am. Chem. Soc.* 125, 6602 (2003).

133. J. D. Mendelsohn, C. J. Barrett, V. V. Chan, A. J. Pal, A. M. Mayes, and M. F. Rubner, *Langmuir* 16, 5017 (2000).
134. A. A. Antipov, G. B. Sukhorukov, and H. Möhwald, *Langmuir* 19, 2444 (2003).
135. R. A. McAloney, V. Dudnik, and M. C. Goh, *Langmuir* 19, 3947 (2003).
136. S. Dragan, S. Schwarz, K.-J. Eichhorn, and K. Lunkwitz, *Colloids Surf. A* 195, 243 (2003).
137. J. Cho, K. Char, J.-D. Hong, and K.-B. Lee, *Adv. Mater.* 13, 1076 (2001).
138. S.-S. Lee, J.-D. Hong, C. H. Kim, K. Kim, J. P. Koo, and K.-B. Lee, *Macromolecules* 34, 5358 (2001).
139. P. A. Chiarelli, M. S. Johal, J. L. Casson, J. B. Roberts, J. M. Robinson, and H.-L. Wang, *Adv. Mater.* 13, 1167 (2001).
140. S.-S. Lee, K.-B. Lee, and J.-D. Hong, *Langmuir* 19, 7592 (2003).
141. G. B. Sukhorukov, E. Donath, H. Lichtenfeld, E. Knippel, M. Knippel, A. Budde, and H. Möhwald, *Colloids Surf. A* 137, 253 (1998).
142. F. Caruso, *Adv. Mater.* 13, 11 (2001).
143. G. B. Sukhorukov, E. Donath, S. Davis, H. Lichtenfeld, F. Caruso, V. I. Popov, and H. Möhwald, *Polym. Adv. Technol.* 9, 759 (1998).
144. O. Mermut and C. J. Barrett, *Analyst* 126, 1861 (2001).
145. L. Richert, P. Lavallo, D. Vautier, B. Senger, J.-F. Stoltz, P. Schaaf, J.-C. Voegel, and C. Picart, *Biomacromolecules* 3, 1170 (2002).
146. W. Jin, X. Shi, and F. Caruso, *J. Am. Chem. Soc.* 123, 8121 (2001).
147. A. Diaspro, D. Silvano, S. Krol, O. Cavalleri, and A. Gliozzi, *Langmuir* 18, 5047 (2002).
148. B. Thierry, F. M. Winnik, Y. Merhi, and M. Tabrizian, *J. Am. Chem. Soc.* 125, 7494 (2003).
149. J.-A. He, S. Bian, L. Li, J. Kumar, S. K. Tripathy, and L. A. Samuelson, *J. Phys. Chem. B* 104, 10513 (2000).
150. S. Balasubramanian, X. Wang, H. C. Wang, K. Yang, J. Kumar, S. K. Tripathy, and L. Li, *Chem. Mater.* 10, 1554 (1998).
151. S. E. Burke and C. J. Barrett, *Biomacromolecules* 4, 1773 (2003).
152. F. Caruso and H. Möhwald, *J. Am. Chem. Soc.* 121, 6039 (1999).
153. Y. Lvov, K. Ariga, M. Onda, I. Ichinose, and T. Kunitake, *Langmuir* 13, 6195 (1997).
154. N. A. Kotov, I. Dekany, and J. H. Fendler, *J. Phys. Chem.* 99, 13065 (1995).
155. E. R. Kleinfeld and G. S. Ferguson, *Science* 265, 370 (1994).
156. Z. Tang, N. A. Kotov, S. Magonov, and B. Ozturk, *Nat. Mater.* 2, 413 (2003).
157. S. Watanabe and S. L. Regen, *J. Am. Chem. Soc.* 116, 8855 (1994).
158. H. Mattoussi, M. F. Rubner, F. Zhou, J. Kumar, and S. K. Tripathy, *Appl. Phys. Lett.* 77, 1540 (2000).
159. J. H. Rouse and G. S. Ferguson, *Langmuir* 18, 7635 (2002).
160. R. C. Advincula, E. Fells, and M.-K. Park, *Chem. Mater.* 13, 2870 (2001).
161. R. C. Advincula, in "Handbook of Polyelectrolytes and their Applications" (S. K. Tripathy, J. Kumar, and H. S. Nalwa, Eds.), Vol. 1, pp. 65–97, American Scientific Publishers, Stevenson Ranch, CA, 2002.
162. J. Ishikawa, A. Baba, F. Kaneko, K. Shinbo, K. Kato, and R. C. Advincula, *Colloids Surf. A* 198–200, 917 (2002).
163. R. Advincula, M.-K. Park, A. Baba, and F. Kaneko, *Langmuir* 19, 654 (2003).
164. S.-H. Lee, S. Balasubramanian, D. Y. Kim, N. K. Viswanathan, S. Bian, J. Kumar, and S. K. Tripathy, *Macromolecules* 33, 6534 (2000).
165. F. Saremi and B. Tieke, *Adv. Mater.* 10, 389 (1998).
166. A. Toutianoush, F. Saremi, and B. Tieke, *Mater. Sci. Eng. C* C8–C9, 343 (1999).
167. A. Toutianoush and B. Tieke, *Macromol. Rapid Commun.* 19, 591 (1998).
168. A. Ziegler, J. Stumpe, A. Toutianoush, and B. Tieke, *Colloids Surf. A* 198–200, 777 (2002).
169. K. E. Van Cott, M. Guzy, P. Neyman, C. Brands, J. R. Heflin, H. W. Gibson, and R. M. Davis, *Angew. Chem. Int. Ed.* 41, 3236 (2002).
170. O. Mermut and C. J. Barrett, *J. Phys. Chem. B* 107, 2525 (2003).
171. O. Mermut, J. Lefebvre, D. G. Gray, and C. J. Barrett, *Macromolecules* 36, 8819 (2003).
172. I. Suzuki, K. Sato, M. Koga, Q. Chen, and J.-I. Anzai, *Mater. Sci. Eng.: C* 23, 579 (2003).
173. L. Wu, X. Tuo, H. Cheng, Z. Chen, and X. Wang, *Macromolecules* 34, 8005 (2001).
174. J.-D. Hong, B.-D. Jung, C. H. Kim, and K. Kim, *Macromolecules* 33, 7905 (2000).
175. B.-D. Jung, J.-D. Hong, A. Voigt, S. Leporatti, L. Dähne, E. Donath, and H. Möhwald, *Colloids Surf. A* 198, 483 (2002).
176. X. Wang, S. Balasubramanian, J. Kumar, S. K. Tripathy, and L. Li, *Chem. Mater.* 10, 1546 (1998).
177. H. Wang, Y. He, X. Tuo, and X. Wang, *Macromolecules* 37, 135 (2004).
178. M.-K. Park and R. C. Advincula, *Langmuir* 18, 4532 (2002).
179. S. Bian, J.-A. He, L. Li, J. Kumar, and S. K. Tripathy, *Adv. Mater.* 12, 1202 (2000).
180. D. S. dos Santos, Jr., A. Bassi, J. J. Rodrigues, Jr., L. Misoguti, O. N. Oliveira, Jr., and C. R. Mendonça, *Biomacromolecules* 4, 1502 (2003).
181. J.-A. He, S. Bian, L. Li, J. Kumar, S. K. Tripathy, and L. A. Samuelson, *Appl. Phys. Lett.* 76, 3233 (2000).
182. S. Dante, R. C. Advincula, C. W. Frank, and P. Stroeve, *Langmuir* 15, 193 (1999).
183. L. Zhai, F. Ç. Cebeci, R. E. Cohen, and M. F. Rubner, *Nano Lett.* 4, 1349 (2004).
184. D. Nyamjav and A. Ivanisevic, *Chem. Mater.* 16, 5216 (2004).
185. A. Natansohn and P. Rochon, *Chem. Rev.* 102, 4139 (2002).
186. P. Uznanski, M. Kryszewski, and E. W. Thulstrup, *Eur. Polym. J.* 27, 41 (1991).
187. J. J. de Lange, J. M. Robertson, and I. Woodward, *Proc. R. Soc.* A171, 398 (1939).

188. G. C. Hampson and J. M. Robertson, *J. Chem. Soc. Abstr.* 409 (1941).
189. C. J. Brown, *Acta Crystallogr.* 21, 146 (1966).
190. T. Naito, K. Horie, and I. Mita, *Polymer* 34, 4140 (1993).
191. R. G. Weiss, V. Ramamurthy, and G. S. Hammond, *Acc. Chem. Res.* 25, 530 (1993).
192. T. Hugel, N. B. Holland, A. Cattani, L. Moroder, M. Seitz, and H. E. Gaub, *Science* 296, 1103 (2002).
193. N. B. Holland, T. Hugel, G. Neuert, A. Cattani-Scholze, C. Renner, D. Oesterhelt, L. Moroder, M. Seitz, and H. E. Gaub, *Macromolecules* 36, 2015 (2003).
194. M. Asakawa, P. R. Ashton, V. Balzani, C. L. Brown, A. Credi, O. A. Matthews, S. P. Newton, F. M. Raymo, A. N. Shipway, N. Spencer, A. Quick, J. F. Stoddart, A. J. P. White, and D. J. Williams, *Chem. Eur. J.* 5, 860 (1999).
195. V. Balzani, A. Credi, F. Marchioni, and J. F. Stoddart, *Chem. Commun.* 18, 1860 (2001).
196. S. Tsuchiya, *J. Am. Chem. Soc.* 121, 48 (1999).
197. C. Steinem, A. Janshoff, M. S. Vollmer, and M. R. Ghadiri, *Langmuir* 15, 3956 (1999).
198. M. S. Vollmer, T. D. Clark, C. Steinem, and M. R. Ghadiri, *Angew. Chem. Int. Ed.* 38, 1598 (1999).
199. K. Ichimura and M. Han, *Chem. Lett.* 29, 286 (2000).
200. A. Natansohn, P. Rochon, M. Pezolet, P. Audet, D. Brown, and S. To, *Macromolecules* 27, 2580 (1994).
201. R. Hagen and T. Bieringer, *Adv. Mater.* 13, 1805 (2001).
202. K. Tawa and W. Knoll, *Macromolecules* 35, 7018 (2002).
203. D. K. Hore, A. Natansohn, and P. L. Rochon, *J. Phys. Chem. B* 106, 9004 (2002).
204. Z. Sekkat, J. Wood, and W. Knoll, *J. Phys. Chem.* 99, 17226 (1995).
205. T. Buffeteau, F. L. Labarthe, M. Pérolet, and C. Sourisseau, *Macromolecules* 34 (2001).
206. D. K. Hore, A. L. Natansohn, and P. L. Rochon, *J. Phys. Chem. B* 107, 2197 (2003).
207. N. C. R. Holme, P. S. Ramanujam, and S. Hvilsted, *Opt. Lett.* 21, 902 (1996).
208. T. S. Lee, D.-Y. Kim, X. L. Jiang, L. Li, J. Kumar, and S. Tripathy, *J. Polym. Sci. Part A: Polym. Chem.* 36, 283 (1998).
209. Z.-S. Xu, V. Drnoyan, A. Natansohn, and P. Rochon, *J. Polym. Sci. Part A: Polym. Chem.* 38, 2245 (2000).
210. Y. Wu, A. Natansohn, and P. Rochon, *Macromolecules* 34, 7822 (2001).
211. R. Hildebrandt, M. Hegelich, H.-M. Keller, G. Marowsky, S. Hvilsted, N. C. R. Holme, and P. S. Ramanujam, *Phys. Rev. Lett.* 81, 5548 (1998).
212. V. Cimrová, D. Neher, R. Hildebrandt, M. Hegelich, A. von der Lieth, G. Marowsky, R. Hagen, S. Kostromine, and T. Bieringer, *Appl. Phys. Lett.* 81, 1228 (2002).
213. Y. Shi, W. H. Steier, L. Yu, M. Chen, and L. R. Dalton, *Appl. Phys. Lett.* 59, 2935 (1991).
214. A. Natansohn and P. Rochon, *Adv. Mater.* 11, 1387 (1999).
215. Y. Shi, W. H. Steier, L. Yu, M. Chen, and L. R. Dalton, *Appl. Phys. Lett.* 58, 1131 (1991).
216. O. Watanabe, M. Tsuchimori, and A. Okada, *J. Mater. Chem.* 6, 1487 (1996).
217. A. Shishido, O. Tsutsumi, A. Kanazawa, T. Shiono, T. Ikeda, and N. Tamai, *J. Am. Chem. Soc.* 119, 7791 (1997).
218. H. J. Eichler, S. Orlic, R. Schulz, and J. Rübner, *Opt. Lett.* 26, 581 (2001).
219. J. J. A. Couture and R. A. Lessard, *Appl. Opt.* 27, 3368 (1988).
220. L. Nikolova, T. Todorov, M. Ivanov, F. Andruzzi, S. Hvilsted, and P. S. Ramanujam, *Appl. Opt.* 35, 3835 (1996).
221. T. Yamamoto, A. Ohashi, S. Yoneyama, M. Hasegawa, O. Tsutsumi, A. Kanazawa, T. Shiono, and T. Ikeda, *J. Phys. Chem. B* 105, 2308 (2001).
222. D. F. Eaton, *Science* 253, 281 (1991).
223. D. M. Burland, R. D. Miller, and C. A. Walsh, *Chem. Rev.* 94, 31 (1994).
224. L. R. Dalton, A. W. Harper, R. Ghosn, W. H. Steier, M. Ziari, H. Fetterman, Y. Shi, R. V. Mustacich, A. K.-Y. Jen, and K. J. Shea, *Chem. Mater.* 7, 1060 (1995).
225. S. K. Yesodha, C. K. S. Pillai, and N. Tsutsumi, *Prog. Polym. Sci.* 29, 45 (2004).
226. D. Brown, A. Natansohn, and P. Rochon, *Macromolecules* 28, 6116 (1995).
227. X. Meng, A. Natansohn, C. Barrett, and P. Rochon, *Macromolecules* 29, 946 (1996).
228. P. M. Blanchard and G. R. Mitchell, *Appl. Phys. Lett.* 63, 2038 (1993).
229. P. M. Blanchard and G. R. Mitchell, *J. Phys. D: Appl. Phys.* 26, 500 (1993).
230. Z. Sekkat, C.-S. Kang, E. F. Aust, G. Wegner, and W. Knoll, *Chem. Mater.* 7, 142 (1995).
231. X. L. Jiang, L. Li, J. Kumar, and S. K. Tripathy, *Appl. Phys. Lett.* 69, 3629 (1996).
232. J.-M. Nunzi, C. Fiorini, A.-C. Etilé, and F. Kajzar, *Pure Appl. Opt.* 7 (1998).
233. X. Zhong, X. Yu, Q. Li, S. Luo, Y. Chen, Y. Sui, and J. Yin, *Opt. Commun.* 190, 333 (2001).
234. S. Yokoyama, T. Nakahama, A. Otomo, and S. Mashiko, *J. Am. Chem. Soc.* 122, 3174 (2000).
235. H. Yamane, H. Kikuchi, and T. Kajiyama, *Polymer* 40, 4777 (1999).
236. C. Barrett, B. Choudhury, A. Natansohn, and P. Rochon, *Macromolecules* 31, 4845 (1998).
237. G. Iftime, F. L. Labarthe, A. Natansohn, P. Rochon, and K. Murti, *Macromolecules* 14, 168 (2002).
238. D. V. Steenwinckel, E. Hendrickx, and A. Persoons, *Chem. Mater.* 14, 1230 (2001).
239. S. K. Prasad and G. G. Nair, *Adv. Mater.* 13, 40 (2001).
240. C. Ruslim and K. Ichimura, *Adv. Mater.* 13, 37 (2001).
241. L. Nikolova, T. Todorov, M. Ivanov, F. Andruzzi, S. Hvilsted, and P. S. Ramanujam, *Opt. Mater.* 8, 255 (1997).
242. M. Ivanov, I. Naydenova, T. Todorov, L. Nikolova, T. Petrova, N. Tomova, and V. Dragostinova, *J. Mod. Opt.* 47, 861 (2000).
243. L. Nikolova, L. Nedelchev, T. Todorov, T. Petrova, N. Tomova, V. Dragostinova, P. S. Ramanujam, and S. Hvilsted, *Appl. Phys. Lett.* 77, 657 (2000).

244. E. Sackmann, *J. Am. Chem. Soc.* 93, 7088 (1971).
245. H. Yamamoto and A. Nishida, *Polym. Int.* 24, 145 (1991).
246. A. Fissi, O. Pieroni, E. Balestreri, and C. Amato, *Macromolecules* 29, 4680 (1996).
247. G. J. Everlof and G. D. Jaycox, *Polymer* 41, 6527 (2000).
248. H. Asanuma, X. Liang, T. Yoshida, and M. Komiyama, *Chem. Bio. Chem.* 2, 39 (2001).
249. W.-S. Lee and A. Ueno, *Macromol. Rapid Commun.* 22, 448 (2001).
250. K. i. Aoki, M. Nakagawa, and K. Ichimura, *J. Am. Chem. Soc.* 122, 10997 (2000).
251. H. Yamamoto, A. Nishida, T. Takimoto, and A. Nagai, *J. Polym. Sci., Part A: Polym. Chem.* 28, 67 (1990).
252. K. Arai and Y. Kawabata, *Macromol. Rapid Commun.* 16, 875 (1995).
253. T. D. Ebralidze and A. N. Mumladze, *Appl. Opt.* 29, 446 (1990).
254. J. J. Effing and J. C. T. Kwak, *Angew. Chem., Int. Ed. Engl.* 34, 88 (1995).
255. L. Yang, N. Takisawa, T. Hayashita, and K. Shirahama, *J. Phys. Chem.* 99, 8799 (1995).
256. M. Higuchi, N. Minoura, and T. Kinoshita, *Chem. Lett.* 227 (1994).
257. M. Higuchi, N. Minoura, and T. Kinoshita, *Macromolecules* 28, 4981 (1995).
258. L. Angiolini, D. Caretti, C. Carlini, and E. Salatelli, *Macromol. Chem. Phys.* 196, 2737 (1995).
259. J. P. Chen, J. P. Gao, and Z. Y. Wang, *J. Polym. Sci., Part A: Polym. Chem.* 35, 9 (1997).
260. M. Sisido, Y. Ishikawa, K. Itoh, and S. Tazuke, *Macromolecules* 24, 3993 (1991).
261. G. Maxein and R. Zentel, *Macromolecules* 28, 8438 (1995).
262. M. Müller and R. Zentel, *Macromolecules* 29, 1609 (1996).
263. M. Higuchi, N. Minoura, and T. Kinoshita, *Colloid Polym. Sci.* 273, 1022 (1995).
264. L. M. Siewierski, W. J. Brittain, S. Petrash, and M. D. Foster, *Langmuir* 12, 5838 (1996).
265. B. Stiller, G. Knochenhauer, E. Markava, D. Gustina, I. Muzikante, P. Karageorgiev, and L. Brehmer, *Mater. Sci. Eng.: C* 8, 385 (1999).
266. C. L. Feng, Y. J. Zhang, J. Jin, Y. L. Song, L. Y. Xie, G. R. Qu, L. Jiang, and D. B. Zhu, *Langmuir* 17, 4593 (2001).
267. G. Moller, M. Harke, H. Motschmann, and D. Prescher, *Langmuir* 14, 4955 (1998).
268. K. Ichimura, S.-K. Oh, and M. Nakagawa, *Science* 288, 1624 (2000).
269. T. Fujita, N. Iyi, and Z. Klapysa, *Mater. Res. Bull.* 33, 1693 (1998).
270. T. Fujita, N. Iyi, and Z. Klapysa, *Mater. Res. Bull.* 36, 557 (2001).
271. M. Ivanov, T. Todorov, L. Nikolova, N. Tomova, and V. Dragostinova, *Appl. Phys. Lett.* 66, 2174 (1995).
272. G. Kleideiter, Z. Sekkat, M. Kreiter, M. D. Lechner, and W. Knoll, *J. Mol. Struct.* 521, 167 (2000).
273. C. D. Eisenbach, *Polymer* 21, 1175 (1980).
274. J. Algers, P. Sperr, W. Egger, L. Liszky, G. Kogel, J. de Baerdemaeker, and F. H. J. Maurer, *Macromolecules* 37, 8035 (2004).
275. Y. Yu, M. Nakano, and T. Ikeda, *Nature* 425, 145 (2003).
276. T. Ikeda, M. Nakano, Y. Yu, O. Tsutsumi, and A. Kanazawa, *Adv. Mater.* 15, 201 (2003).
277. D. Bublit, M. Helgert, B. Fleck, L. Wenke, S. Hvilsted, and P. S. Ramanujam, *Appl. Phys. B: Lasers Opt.* 70, 863 (2000).
278. H. F. Ji, Y. Feng, X. H. Xu, V. Purushotham, T. Thundat, and G. M. Brown, *Chem. Commun.* 2532 (2004).
279. S. Bai and Y. Zhao, *Macromolecules* 34, 9032 (2001).
280. S. H. Barley, A. Gilbert, and G. R. Mitchell, *J. Mater. Chem.* 1, 481 (1991).
281. K. Sumaru, S. Inui, and T. Yamanaka, *Opt. Eng.* 38, 274 (1999).
282. J.-I. Anzai and T. Osa, *Tetrahedron* 50, 4039 (1994).
283. I. Willner and B. Willner, *Adv. Mater.* 9, 351 (1997).
284. H. Tokuhisa, M. Yokoyama, and K. Kimura, *Macromolecules* 27, 1842 (1994).
285. I. Zawisza, R. Bilewicz, E. Luboch, and J. F. Biernat, *Thin Solid Films* 348, 173 (1999).
286. N. Reynier, J.-F. Dozol, M. Saadioui, Z. Asfari, and J. Vicens, *Tetrahedron Lett.* 39, 6461 (1998).
287. K. Kano, Y. Tanaka, T. Ogawa, M. Shimoura, Y. Okahata, and T. Kunitake, *Chem. Lett.* 421 (1980).
288. G. Abraham and E. Purushothaman, *Indian J. Chem. Technol.* 5, 213 (1998).
289. T. Sata, Y. Shimokawa, and K. Matsusaki, *J. Membr. Sci.* 171, 31 (2000).
290. N. Liu, D. R. Dunphy, P. Atanassov, S. D. Bunge, Z. Chen, G. P. López, T. J. Boyle, and C. J. Brinker, *Nano Lett.* 4, 551 (2004).
291. L. Lien, D. C. J. Jaikaran, Z. Zhang, and G. A. Woolley, *J. Am. Chem. Soc.* 118, 12222 (1996).
292. F. Wuerthner and J. Rebek, Jr., *Angew. Chem., Int. Ed. Engl.* 34, 446 (1995).
293. N. Minoura, K. Idei, A. Rachkov, Y.-W. Choi, M. Ogiso, and K. Matsuda, *Macromolecules* 37, 9571 (2004).
294. P. Uznanski and J. Pecherz, *J. Appl. Polym. Sci.* 86, 1459 (2002).
295. H. Yamamoto, *Macromolecules* 19, 2472 (1986).
296. S. Spörlein, H. Carstens, H. Satzger, C. Renner, R. Behrendt, L. Moroder, P. Tavan, W. Zinth, and J. Wachtveitl, *Proc. Natl. Acad. Sci. USA* 99, 7998 (2002).
297. J. Bredenbeck, J. Helbing, R. Behrendt, C. Renner, L. Moroder, J. Wachtveitl, and P. Hamm, *J. Phys. Chem. B* 107, 8654 (2003).
298. Z. F. Liu, K. Hashimoto, and A. Fujishima, *Nature* 347, 658 (1990).
299. A. Dhanabalan, D. S. Dos Santos, Jr., C. R. Mendonça, L. Misoguti, D. T. Balogh, J. A. Giacometti, S. C. Zilio, and O. N. Oliveira, Jr., *Langmuir* 15, 4560 (1999).
300. Y. Sabi, M. Yamamoto, H. Watanabe, T. Bieringer, D. Haarer, R. Hagen, S. G. Kostromine, and H. Berneth, *Jpn. J. Appl. Phys., Part 1* 40, 1613 (2001).

301. M. Ishikawa, Y. Kawata, C. Egami, O. Sugihara, N. Okamoto, M. Tsuchimori, and O. Watanabe, *Opt. Lett.* 23, 1781 (1998).
302. S. Kawata and Y. Kawata, *Chem. Rev.* 100, 1777 (2000).
303. P. S. Ramanujam, S. Hvilsted, F. Ujhelyi, P. Koppa, E. Lörincz, G. Erdei, and G. Szarvas, *Synth. Met.* 124, 145 (2001).
304. S. J. Zilker, T. Bieringer, D. Haarer, R. S. Stein, J. W. van Egmond, and S. G. Kostromine, *Adv. Mater.* 10, 855 (1998).
305. R. H. Berg, S. Hvilsted, and P. S. Ramanujam, *Nature* 383, 505 (1996).
306. P. Rochon, E. Batalla, and A. Natansohn, *Appl. Phys. Lett.* 66, 136 (1995).
307. D. Y. Kim, S. K. Tripathy, L. Li, and J. Kumar, *Appl. Phys. Lett.* 66, 1166 (1995).
308. S. Yamaki, M. Nakagawa, S. Morino, and K. Ichimura, *Appl. Phys. Lett.* 76, 2520 (2000).
309. K. G. Yager and C. J. Barrett, *Curr. Opin. Solid State Mater. Sci.* 5, 487 (2001).
310. D. Y. Kim, L. Li, X. L. Jiang, V. Shivshankar, J. Kumar, and S. K. Tripathy, *Macromolecules* 28, 8835 (1995).
311. C. J. Barrett, A. L. Natansohn, and P. L. Rochon, *J. Phys. Chem.* 100, 8836 (1996).
312. S. P. Bian, J. M. Williams, D. Y. Kim, L. A. Li, S. Balasubramanian, J. Kumar, and S. Tripathy, *J. Appl. Phys.* 86, 4498 (1999).
313. T. Fukuda, H. Matsuda, T. Shiraga, T. Kimura, M. Kato, N. K. Viswanathan, J. Kumar, and S. K. Tripathy, *Macromolecules* 33, 4220 (2000).
314. C. Sanchez, R. Alcalá, S. Hvilsted, and P. S. Ramanujam, *Appl. Phys. Lett.* 77, 1440 (2000).
315. C. Jager, T. Bieringer, and S. J. Zilker, *Appl. Opt.* 40, 1776 (2001).
316. D. Y. Kim, T. S. Lee, S. K. Tripathy, X. L. Jiang, L. Li, and J. Kumar, *Macromol. Symp.* 116, 127 (1997).
317. J. Kumar, L. Li, X. L. Jiang, D. Y. Kim, T. S. Lee, and S. Tripathy, *Appl. Phys. Lett.* 72, 2096 (1998).
318. S. Bian, L. Li, J. Kumar, D. Y. Kim, J. Williams, and S. K. Tripathy, *Appl. Phys. Lett.* 73, 1817 (1998).
319. N. C. R. Holme, L. Nikolova, S. Hvilsted, P. H. Rasmussen, R. H. Berg, and P. S. Ramanujam, *Appl. Phys. Lett.* 74, 519 (1999).
320. M. Helgert, L. Wenke, S. Hvilsted, and P. S. Ramanujam, *Appl. Phys. B: Lasers Opt.* 72, 429 (2001).
321. N. Zettsu, T. Fukuda, H. Matsuda, and T. Seki, *Appl. Phys. Lett.* 83, 4960 (2003).
322. I. Naydenova, L. Nikolova, T. Todorov, N. C. R. Holme, P. S. Ramanujam, and S. Hvilsted, *J. Opt. Soc. Am. B* 15, 1257 (1998).
323. F. L. Labarthe, J. L. Bruneel, T. Buffeteau, C. Sourisseau, M. R. Huber, S. J. Zilker, and T. Bieringer, *Phys. Chem. Chem. Phys.* 2, 5154 (2000).
324. F. L. Labarthe, T. Buffeteau, and C. Sourisseau, *J. Appl. Phys.* 90, 3149 (2001).
325. F. Lagugne-Labarthe, J. L. Bruneel, V. Rodriguez, and C. Sourisseau, *J. Phys. Chem. B* 108, 1267 (2004).
326. R. D. Schaller, R. J. Saykally, Y. R. Shen, and F. Lagugne-Labarthe, *Opt. Lett.* 28, 1296 (2003).
327. X. L. Jiang, J. Kumar, D. Y. Kim, V. Shivshankar, and S. K. Tripathy, *Appl. Phys. Lett.* 68, 2618 (1996).
328. N. K. Viswanathan, S. Balasubramanian, L. Li, S. K. Tripathy, and J. Kumar, *Jpn. J. Appl. Phys.* 38, 5928 (1999).
329. X. L. Jiang, L. Li, J. Kumar, D. Y. Kim, and S. K. Tripathy, *Appl. Phys. Lett.* 72, 2502 (1998).
330. F. Lagugne-Labarthe, T. Buffeteau, and C. Sourisseau, *Phys. Chem. Chem. Phys.* 4, 4020 (2002).
331. F. L. Labarthe, J. L. Bruneel, T. Buffeteau, and C. Sourisseau, *J. Phys. Chem. B* 108, 6949 (2004).
332. O. Henneberg, T. Geue, U. Pietsch, M. Saphiannikova, and B. Winter, *Appl. Phys. Lett.* 84, 1561 (2004).
333. U. Pietsch, P. Rochon, and A. Natansohn, *Adv. Mater.* 12, 1129 (2000).
334. T. Geue, O. Henneberg, J. Grenzer, U. Pietsch, A. Natansohn, P. Rochon, and K. Finkelstein, *Colloid Surf. A* 198–200, 31 (2002).
335. T. M. Geue, M. G. Saphiannikova, O. Henneberg, U. Pietsch, P. L. Rochon, and A. L. Natansohn, *J. Appl. Phys.* 93, 3161 (2003).
336. U. Pietsch, *Phys. Rev. B* 66, 155 430 (2002).
337. O. Watanabe, T. Ikawa, M. Hasegawa, M. Tsuchimori, Y. Kawata, C. Egami, O. Sugihara, and N. Okamoto, *Mol. Cryst. Liq. Cryst.* 345, 629 (2000).
338. T. Ikawa, T. Mitsuoka, M. Hasegawa, M. Tsuchimori, O. Watanabe, Y. Kawata, C. Egami, O. Sugihara, and N. Okamoto, *J. Phys. Chem. B* 104, 9055 (2000).
339. C. D. Keum, T. Ikawa, M. Tsuchimori, and O. Watanabe, *Macromolecules* 36, 4916 (2003).
340. S. Z. Yang, L. Li, A. L. Cholli, J. Kumar, and S. K. Tripathy, *J. Macromol. Sci. Pure* 38, 1345 (2001).
341. S. Yang, M. M. Jacob, L. Li, K. Yang, A. L. Cholli, J. Kumar, and S. K. Tripathy, *Polym. News* 27, 368 (2002).
342. S. Z. Yang, L. Li, A. L. Cholli, J. Kumar, and S. K. Tripathy, *Biomacromolecules* 4, 366 (2003).
343. H. Nakano, T. Takahashi, T. Kadota, and Y. Shirota, *Adv. Mater.* 14, 1157 (2002).
344. H. Ando, T. Takahashi, H. Nakano, and Y. Shirota, *Chem. Lett.* 32, 710 (2003).
345. F. Ciuchi, A. Mazzulla, and G. Cipparrone, *J. Opt. Soc. Am. B* 19, 2531 (2002).
346. I. Naydenova, T. Petrova, N. Tomova, V. Dragostinova, L. Nikolova, and T. Todorov, *Pure Appl. Opt.* 7, 723 (1998).
347. T. Ubukata, T. Seki, and K. Ichimura, *Adv. Mater.* 12, 1675 (2000).
348. T. Ubukata, T. Seki, and K. Ichimura, *Colloid Surf. A* 198, 113 (2002).
349. P. S. Ramanujam, N. C. R. Holme, and S. Hvilsted, *Appl. Phys. Lett.* 68, 1329 (1996).
350. A. Archut, F. Vögtle, L. D. Cola, G. C. Azzellini, V. Balzani, P. S. Ramanujam, and R. H. Berg, *Chem.–Eur. J.* 4, 699 (1998).
351. L. Andruzzi, A. Altomare, F. Ciardelli, R. Solaro, S. Hvilsted, and P. S. Ramanujam, *Macromolecules* 32, 448 (1999).

352. A. Natansohn, S. Xie, and P. Rochon, *Macromolecules* 25, 5531 (1992).
353. M. S. Ho, A. Natansohn, and P. Rochon, *Macromolecules* 28, 6124 (1995).
354. J. P. Chen, F. L. Labarthe, A. Natansohn, and P. Rochon, *Macromolecules* 32, 8572 (1999).
355. Y. L. Wu, A. Natansohn, and P. Rochon, *Macromolecules* 34, 7822 (2001).
356. N. K. Viswanathan, S. Balasubramanian, L. Li, J. Kumar, and S. K. Tripathy, *J. Phys. Chem. B* 102, 6064 (1998).
357. T. M. Geue, A. G. Saphiannikova, O. Henneberg, U. Pietsch, P. L. Rochon, and A. L. Natansohn, *Phys. Rev. E* 65, 052801 (2002).
358. M. Kameda, K. Sumaru, T. Kanamori, and T. Shinbo, *J. Appl. Polym. Sci.* 88, 2068 (2003).
359. L. Sharma, T. Matsuoka, T. Kimura, and H. Matsuda, *Polym. Adv. Technol.* 13, 481 (2002).
360. K. Yang, S. Z. Yang, X. G. Wang, and J. Kumar, *Appl. Phys. Lett.* 84, 4517 (2004).
361. G. S. Kumar, P. DePra, K. Zhang, and D. C. Neckers, *Macromolecules* 17, 2463 (1984).
362. A. Bhatnagar, J. Mueller, D. J. Osborn, T. L. Martin, J. Wirtz, and D. K. Mohanty, *Polymer* 36, 3019 (1995).
363. M. Moniruzzaman, C. J. Sabey, and G. F. Fernando, *Macromolecules* 37, 2572 (2004).
364. J. A. Forrest and K. Dalnoki-Veress, *Adv. Colloid Interface Sci.* 94, 167 (2001).
365. T. Sriksirin, A. Laschitsch, D. Neher, and D. Johannsmann, *Appl. Phys. Lett.* 77, 963 (2000).
366. N. Mechau, D. Neher, V. Borger, H. Menzel, and K. Urayama, *Appl. Phys. Lett.* 81, 4715 (2002).
367. B. Stiller, P. Karageorgiev, T. Geue, K. Morawetz, M. Saphiannikova, N. Mechau, and D. Neher, *Phys. Low-Dimens. Str.* 1–2, 129 (2004).
368. N. C. R. Holme, L. Nikolova, P. S. Ramanujam, and S. Hvilsted, *Appl. Phys. Lett.* 70, 1518 (1997).
369. F. L. Labarthe, P. Rochon, and A. Natansohn, *Appl. Phys. Lett.* 75, 1377 (1999).
370. M. Helgert, B. Fleck, L. Wenke, S. Hvilsted, and P. S. Ramanujam, *Appl. Phys. B-Lasers O* 70, 803 (2000).
371. T. Geue, O. Henneberg, and U. Pietsch, *Cryst. Res. Technol.* 37, 770 (2002).
372. T. Geue, M. Schultz, J. Grenzer, U. Pietsch, A. Natansohn, and P. Rochon, *J. Appl. Phys.* 87, 7712 (2000).
373. O. Henneberg, T. Geue, M. Saphiannikova, U. Pietsch, P. Rochon, and A. Natansohn, *Appl. Surf. Sci.* 182, 272 (2001).
374. O. Henneberg, T. Geue, P. Rochon, and U. Pietsch, *J. Phys. D Appl. Phys.* 36, A241 (2003).
375. M. Saphiannikova, O. Henneberg, T. M. Gene, U. Pietsch, and P. Rochon, *J. Phys. Chem. B* 108, 15084 (2004).
376. O. Henneberg, T. Geue, M. Saphiannikova, U. Pietsch, L. F. Chi, P. Rochon, and A. L. Natansohn, *Appl. Phys. Lett.* 79, 2357 (2001).
377. A. Stracke, J. H. Wendorff, D. Goldmann, D. Janietz, and B. Stiller, *Adv. Mater.* 12, 282 (2000).
378. N. Kawatsuki, E. Uchida, and H. Ono, *Appl. Phys. Lett.* 83, 4544 (2003).
379. C. J. Barrett, P. L. Rochon, and A. L. Natansohn, *J. Chem. Phys.* 109, 1505 (1998).
380. K. Sumaru, T. Yamanaka, T. Fukuda, and H. Matsuda, *Appl. Phys. Lett.* 75, 1878 (1999).
381. T. Fukuda, K. Sumaru, T. Yamanaka, and H. Matsuda, *Mol. Cryst. Liq. Cryst.* 345, 587 (2000).
382. D. Bublitz, B. Fleck, and L. Wenke, *Appl. Phys. B-Lasers O* 72, 931 (2001).
383. M. Saphiannikova, T. M. Geue, O. Henneberg, K. Morawetz, and U. Pietsch, *J. Chem. Phys.* 120, 4039 (2004).
384. G. Pawlik, A. C. Mitus, A. Miniewicz, and F. Kajzar, *J. Chem. Phys.* 119, 6789 (2003).
385. A. C. Mitus, G. Pawlik, A. Miniewicz, and F. Kajzar, *Mol. Cryst. Liq. Cryst.* 416, 113 (2004).
386. G. Pawlik, A. C. Mitus, A. Miniewicz, and F. Kajzar, *J. Nonlinear Opt. Phys. Mater.* 13, 481 (2004).
387. K. G. Yager and C. J. Barrett, *J. Chem. Phys.* 120, 1089 (2004).
388. K. Schmitt, C. Benecke, and M. Schadt, *Appl. Opt.* 36, 5078 (1997).
389. P. S. Ramanujam, M. Pedersen, and S. Hvilsted, *Appl. Phys. Lett.* 74, 3227 (1999).
390. A. Leopold, J. Wolff, O. Baldus, M. R. Huber, T. Bieringer, and S. J. Zilker, *J. Chem. Phys.* 113, 833 (2000).
391. J. H. Si, J. R. Qiu, J. F. Zhai, Y. Q. Shen, and K. Hirao, *Appl. Phys. Lett.* 80, 359 (2002).
392. O. Baldus, A. Leopold, R. Hagen, T. Bieringer, and S. J. Zilker, *J. Chem. Phys.* 114, 1344 (2001).
393. P. Lefin, C. Fiorini, and J. M. Nunzi, *Opt. Mater.* 9, 323 (1998).
394. P. Lefin, C. Fiorini, and J. M. Nunzi, *Pure Appl. Opt.* 7, 71 (1998).
395. T. G. Pedersen and P. M. Johansen, *Phys. Rev. Lett.* 79, 2470 (1997).
396. T. G. Pedersen, P. M. Johansen, N. C. R. Holme, P. S. Ramanujam, and S. Hvilsted, *Phys. Rev. Lett.* 80, 89 (1998).
397. O. Baldus and S. J. Zilker, *Appl. Phys. B-Lasers O* 72, 425 (2001).
398. S. P. Bian, W. Liu, J. Williams, L. Samuelson, J. Kumar, and S. Tripathy, *Chem. Mater.* 12, 1585 (2000).
399. A. Ashkin, *Phys. Rev. Lett.* 24, 156 (1970).
400. A. Ashkin, *Proc. Natl. Acad. Sci. USA* 94, 4853 (1997).
401. P. C. Chaumet and M. Nieto-Vesperinas, *Opt. Lett.* 25, 1065 (2000).
402. T. Ikawa, T. Mitsuoka, M. Hasegawa, M. Tsuchimori, O. Watanabe, and Y. Kawata, *Phys. Rev. B* 64 (2001).
403. J. P. Gordon, *Phys. Rev. A* 8, 14 (1973).
404. M. Matsumoto, D. Miyazaki, M. Tanaka, R. Azumi, E. Manda, Y. Kondo, N. Yoshino, and H. Tachibana, *J. Am. Chem. Soc.* 120, 1479 (1998).
405. C. Hubert, C. Fiorini-Debuisschert, I. Maurin, J. M. Nunzi, and P. Raimond, *Adv. Mater.* 14, 729 (2002).
406. C. Hubert, E. Malcor, I. Maurin, J. M. Nunzi, P. Raimond, and C. Fiorini, *Appl. Surf. Sci.* 186, 29 (2002).
407. F. Ciuchi, A. Mazzulla, G. Carbone, and G. Cipparrone, *Macromolecules* 36, 5689 (2003).
408. N. Zettsu, T. Ubukata, T. Seki, and K. Ichimura, *Adv. Mater.* 13, 693 (2001).
409. S. K. Tripathy, N. K. Viswanathan, S. Balasubramanian, and J. Kumar, *Polym. Adv. Technol.* 11, 570 (2000).
410. P. Rochon, A. Natansohn, C. L. Callendar, and L. Robitaille, *Appl. Phys. Lett.* 71, 1008 (1997).
411. R. J. Stockermans and P. L. Rochon, *Appl. Opt.* 38, 3714 (1999).

412. J. Paterson, A. Natansohn, P. Rochon, C. L. Callendar, and L. Robitaille, *Appl. Phys. Lett.* 69, 3318 (1996).
413. T. Nagata, T. Matsui, M. Ozaki, K. Yoshino, and F. Kajzar, *Synth. Met.* 119, 607 (2001).
414. V. Dumarcher, L. Rocha, C. Denis, C. Fiorini, J.-M. Nunzi, F. Sobel, B. Sahraoui, and D. Gindre, *J. Opt. A: Pure Appl. Opt.* 2, 279 (2000).
415. L. Rocha, V. Dumarcher, C. Denis, P. Raimond, C. Fiorini, and J. M. Nunzi, *J. Appl. Phys.* 89, 3067 (2001).
416. C. Egami, Y. Kawata, Y. Aoshima, S. Alasfar, O. Sugihara, H. Fujimura, and N. Okamoto, *Jpn. J. Appl. Phys.* 39, 1558 (2000).
417. J. Neumann, K. S. Wiekling, and D. Kip, *Appl. Opt.* 38, 5418 (1999).
418. X. T. Li, A. Natansohn, and P. Rochon, *Appl. Phys. Lett.* 74, 3791 (1999).
419. M.-H. Kim, J.-D. Kim, T. Fukuda, and H. Matsuda, *Liq. Cryst.* 27, 1633 (2000).
420. A. Parfenov, N. Tamaoki, and S. Ohnishi, *J. Appl. Phys.* 87, 2043 (2000).
421. A. Parfenov, N. Tamaoki, and S. Ohni-Shi, *Mol. Cryst. Liq. Cryst.* 359, 487 (2001).
422. F. Kaneko, T. Kato, A. Baba, K. Shinbo, K. Kato, and R. C. Advincula, *Colloid Surf. A* 198, 805 (2002).
423. Y. H. Ye, S. Badilescu, V. V. Truong, P. Rochon, and A. Natansohn, *Appl. Phys. Lett.* 79, 872 (2001).
424. D. K. Yi, M. J. Kim, and D. Y. Kim, *Langmuir* 18, 2019 (2002).
425. D. K. Yi, E.-M. Seo, and D.-Y. Kim, *Langmuir* 18, 5321 (2002).
426. S. Noel, E. Batalla, and P. Rochon, *J. Mater. Res.* 11, 865 (1996).
427. M. Hasegawa, T. Ikawa, M. Tsuchimori, O. Watanabe, and Y. Kawata, *Macromolecules* 34, 7471 (2001).
428. M. Hasegawa, C.-D. Keum, and O. Watanabe, *Adv. Mater.* 14, 1738 (2002).
429. T. Fukuda, K. Sumaru, T. Kimura, H. Matsuda, Y. Narita, T. Inoue, and F. Sato, *Jpn. J. Appl. Phys.* 40, L900 (2001).